UNIVERSITY OF CALIFORNIA

Los Angeles

Predicting Antibiotic Effectiveness Across the Range of Bacterial Diversity

A thesis submitted in partial satisfaction
of the requirements for the degree of Master of Science
in Bioinformatics

by

Shaili Mathur

2021

ABSTRACT OF THE THESIS

Predicting Antibiotic Effectiveness
Across the Range of Bacterial Diversity

by

Shaili Mathur

Master of Science in Bioinformatics
University of California, Los Angeles, 2021
Professor Van M. Savage, Chair

How antibiotic efficacy varies with bacterial species is of basic and applied importance, including understanding of microbial dynamics in clinical and ecological contexts. Cellular components that antibiotics target — DNA, proteins, mRNA, tRNA, cellular envelope, and ribosomes — all scale non-linearly with cell volume. We develop theory that shows how antibiotic efficacy may depend on cell size based on the specific cellular components targeted by the antibiotics and the nonlinearities between those components and cell size. We measure cell size and minimum inhibitory concentrations in 11 bacterial species and 24 antibiotics. We present a detailed model for ribosome-targeting antibiotics through which we can generate dose-response curves and make predictions for minimum inhibitory concentrations based on cell size. We find that energetic and volumetric limitations on cell growth create trade-

offs, leading to the surprising prediction that mid-sized cells are the least susceptible to antibiotics. This finding is matched by our theoretical predictions.

The thesis of Shaili Mathur is approved.

Nandita R. Garud

Pamela J. Yeh

Van M. Savage, Committee Chair

University of California, Los Angeles

2021

To my parents, Shesha and Shobhit,
who have always put me in front of themselves
and continue to teach me to work hard,
to be kind, and to be resilient,
to my grandmother, Ilaben, who was an example in
strength, conviction, and compassion
and was taken away from us too quickly by AMR,
and to my grandfather, Achal, who showed
me the beauty in intellectual pursuits.

Contents

List of Figures

List of Tables

Acknowledgements

There are several people that have made it possible for me to pursue an education at UCLA and to complete this thesis. First and foremost, Professor Van Savage, who has advised me over the last four years with unfailing kindness, generosity, intelligence, and humor – thank you for everything. I am also grateful to Professor Chris Kempes, for his mentorship throughout the course of this project, and especially at the 2019 Santa Fe Institute REU, and to Professor Pamela Yeh, for her support and advice on the experimental side of this project. I would also like to thank my committee members, Professor Van Savage, Professor Pamela Yeh, and Professor Nandita Garud for the time they spent on helping me with this thesis.

I would also like to thank Dr. Portia Mira, whose experience I benefited and learned from while conducting experiments myself, for all of her work in designing the experiments and data collection for this thesis.

I would like to thank my parents, Shesha and Shobhit, for their constant support, and all of the people in my life who have encouraged and inspired me to take on this thesis.

This work was funded in part my the Whitecome Undergraduate Summer Research Fellowship from the UCLA Department of Ecology and Evolutionary Biology, and the Undergraduate Research Fellows Program through the Undergraduate Research Center. I am extremely grateful for their support.

1 Introduction

Antibiotic resistance is anticipated to be one of the most serious challenges for human health worldwide by 2050 [1, 2]. However, we lack a systematic understanding of which bacterial species can be expected to be susceptible to particular antibiotics. Quantitative models of antibiotic dynamics within bacterial cells are needed for such general conclusions and predictions but do not yet exist. A starting point for such models could be to construct them around general cell features such as cell size and known antibiotic mechanisms-of-actions that disrupt essential processes including translation in ribosomes, growth and repair of the cell wall, the function of specific proteins, and genomic repair and replication.

Because bacterial cell size constrains physiological rates and function across species, it can serve as an early measurable property that is a generic indicator of cellular dynamics and potential responses to antibiotics. For instance, molecular transport rates change systematically with size across the cellular envelope (due to surface-area effects), and metabolic and growth rates, protein composition, and the number of required ribosomes all increase–often nonlinearly–with cell volume. These shifts with cell size can often be predicted from fundamental physical constraints such as the total energy available to a cell or the inherent polymerization rate of the ribosome. Previous work has shown that cell size and composition drives energy budgets and metabolic rates across bacterial species [3]. Additionally, Kempes *et al* [4] have shown that nearly all of cellular composition–including the percentage volume of genetic material, tRNA, mRNA, ribosomes, proteins, and the cellular envelope–shifts systematically with cell size across bacterial diversity. Because antibiotics target these components it is possible that cell size has an effect on antibiotic susceptibility. This perspective informs both detailed models of cellular physiology and broad-scale predictions across the range of life.

Indeed, there is empirical evidence that cell size is correlated with antibiotic susceptibility in sub-populations of bacterial strains in a variety of species. Vijay *et al*[5] and Aldrige *et*

al [6] found that Mycobacteria have sub-populations that differ in growth rate and cell size, and that they have different levels of antibiotic susceptibility. Vijay *et al* found that smaller cells are more susceptible to antibiotics including rifampicin and isoniazid, and results from Aldrige *et al* suggest that differences in antibiotic susceptibility driven by cell size depend on antibiotic mechanism of action. Additionally, Song and Ren found a correlation between smaller cell volume and antibiotic susceptibility in *Escherichia coli* and *Pseudomonas aeruginosa* biofilms based on the stiffness of the substrate. It has also been observed that exposure of *Escherichia coli* biofilms to ampicillin and ciprofloxacin increases the mean and variance in cell size distributions (Gomes *et al* [7]), suggesting that increasing cell size could be a phenotypically plastic response to antibiotic stress, or that cells within colonies are differentially susceptible to antibiotics based on cell size.

In order to build a quantitative model of antibiotic susceptibility across bacterial species, we need to connect the molecular dynamics of antibiotics and target components, cell size-driven shifts in cell morphology, and the effects of cellular composition on metabolic and growth rates. Kempes *et al* showed that cell size predicts cellular composition, and there is also a body of work linking cellular composition to growth rates in bacterial species [8]. Both of these perspectives can be combined with a knowledge of antibiotic mechanisms to make quantitative models linking cell size with inhibition of bacterial growth under antibiotic stress.

Cellular composition, which has been shown to be size dependent, has also been connected to growth rates in different environmental conditions [9–11]. Monod suggested the simple principle that all components of the cell double at the same rate by the time of cell division [12] and Schaechter, Maaløe and Kjeldgaard showed the macromolecular composition of Salmonella (mass of RNA, DNA, protein and cell mass itself) is a function of the doubling rate alone across various nutrient media [13]. Greulich *et al* used these principles to model the dynamics of growth inhibition by ribosome-targeting antibiotics by incorporating the

molecular dynamics of diffusion and binding and phenomenological relationships between ribosomal content and growth rate [14], but did not consider the effects of cell size on growth inhibition.

To our knowledge there have been no studies of bacterial species that vary in cell size across several orders of magnitude, or detailed mechanistic models that integrate systematic changes across cell sizes with the dynamics of antibiotics within cells. To make cross-species predictions of antibiotic susceptibility, we build theoretical models that combine an antibiotic's mechanism-of-action with systematic size dependent changes in cellular composition and metabolic rate. We do this by deriving a general model that incorporates diffusion across the cell membrane, molecular dynamics, the cell's energy budget, and volumetric constraints. As a special case of the general model, we construct a detailed model for ribosome-targeting antibiotic. This allows us to calculate and predict dose-response curves with biologically meaningful parameters that match our empirical data, and to make across-species predictions of antibiotic susceptibility.

To test the effects of cell size empirically, we made detailed measurements of dose-response curves in 11 bacterial species of varying cell sizes exposed to 24 antibiotics that span five different mechanisms-of-action: inhibition of protein synthesis, cell wall repair and growth, DNA gyrase, RNA synthesis, folic acid synthesis. A common measure of antibiotic susceptibility is the minimum inhibitory concentration (MIC), the concentration at which 95% of growth is inhibited after 24 hours. We compare experimentally measured MICs of bacterial species of various cell sizes across several antibiotics.

Our theoretical and empirical work suggests that cells have to growth within multiple constraints, including limitations on energetic resources and cell volume. The degree to which cells are limited by these different constraints can shift in opposite directions with cell size, resulting in non-monotonic trends in antibiotic susceptibility across cell size that with "energy-limited" and "volume-limited" regimes in cell size. Indeed, we find in our

theoretical work that there are trade-offs between the two constraints, leading to lower antibiotic susceptibility in mid-sized cells. Furthermore, this surprising theoretical prediction is matched by our experimental work.

2 Theoretical Framework

We now develop a general framework for how to model antibiotic dynamics and how antibiotic susceptibility depends on cell size (schematic in Figure 1). We account for antibiotic diffusion, changes in metabolic rates, energy budget, and volumetric constraints on cellular response to make predictions for responses to antibiotic stress, and generate dose response curves. We use minimum inhibitory concentration (MIC), which is defined as the concentration at which 95% of growth is inhibited at 24 hours as a measure of antibiotic susceptibility. Because this is the value that we measure experimentally, we are able to compare our theoretical predictions directly to experimental results. We then connect our model of antibiotic stress response to cell size dependencies including the surface area effects, shifts in cellular compositions and the energetic costs of growth to make predictions about shifts in MIC across bacterial species of different cell sizes [3, 4, 15, 16].

Our framework consists of a dynamical systems model of the antibiotic, target component, other cellular component(s) that depend directly on the target component, and a model of the cell's energy budget. We (i) find the steady-state internal antibiotic concentration that is driven by both the surface area of the cell membrane and the molecular dynamics of the antibiotic and the target component, which both depends on cell size, (ii) find the optimal scheme for mitigating downstream effects of the antibiotic inhibiting the target component under model constraints and assumptions (by up-regulation or down-regulation of the target component and resource redistribution) (iii) find the energetic costs associated with the cellular response to antibiotics, and (iv) find the minimum time of division under antibiotic

stress which allows the cell to double all of its components, and (v) produce the dose response curve using a logistic growth model. This gives us the MIC based on energetic principles. We also consider the increase in dry mass of a cell due to the build up of non-functional antibiotic-target complexes, and find the "volume-limiting" concentration at which the required dry volume fraction exceeds the total cell volume. The predicted MIC is the minimum of the "energy-liming" and "volume-limiting" antibiotic concentration in the model. The general model that is outlined here is expanded on in the following section, where we derive a detailed model for ribosome-targeting antibiotics.

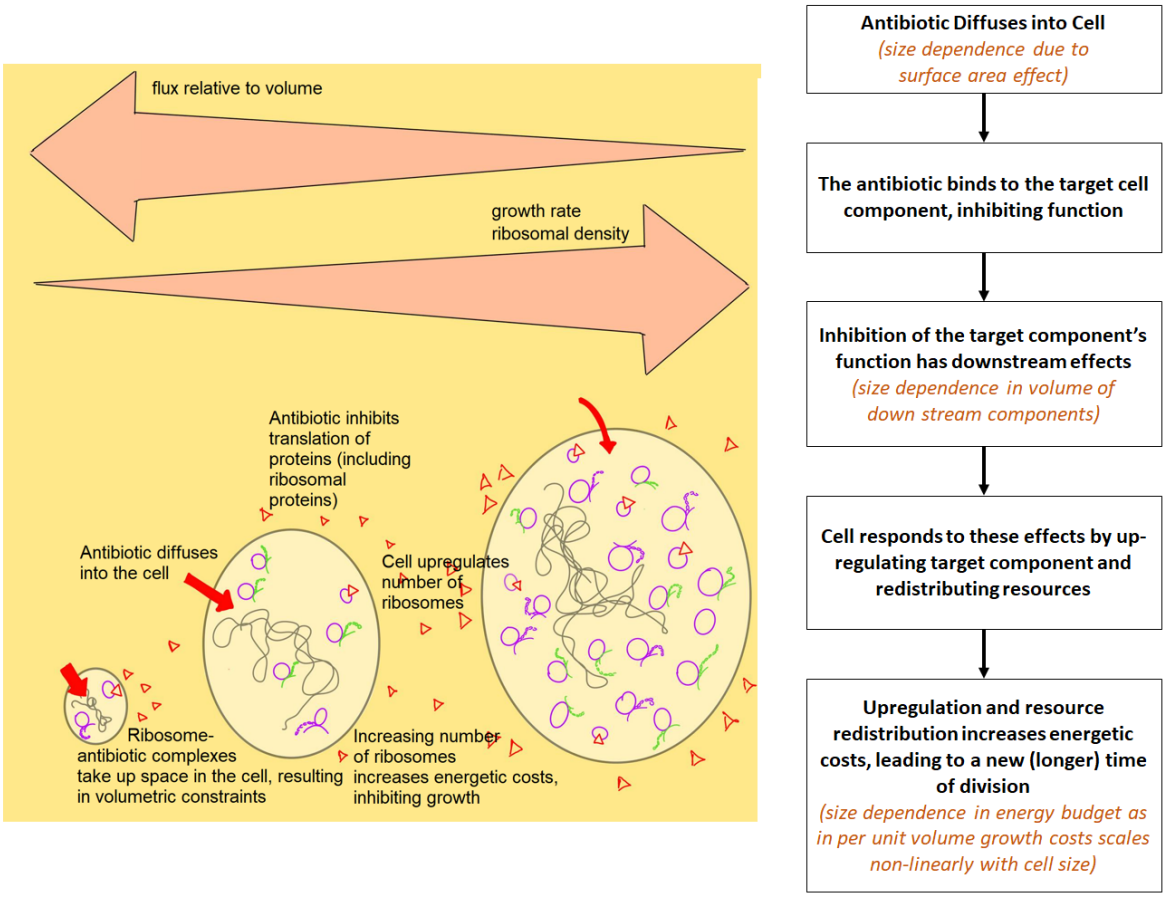

Figure 1: **Schematic of the theoretical framework** Model of a single cell responding to antibiotic stress incorporates diffusion of the antibiotic across the cell membrane, molecular dynamics of the antibiotic and its target, reallocation of resources in the cell, and the energy budget of the cell to produce a dose response curve. Cell size affects the density of the target (ribosomes), flux into the cell, and the cell's energy budget and therefore growth rate. The bacterial cell is modeled as a well-mixed cell that responds optimally to antibiotic stress within these model constrains and assumptions.

2.1 Modeling of Dose Response Curves for Ribosome-Targeting Antibiotics in in Single Cells

We present a model of ribosome targeting antibiotics as a special case of the general framework described above. This model illustrates how the general framework can be used to model antibiotic stress response and make cross-species predictions about antibiotic susceptibility.

2.1.1 Model of Ribosome and Protein Dynamics

We modify the dynamical systems model of the ribosomal and protein pool in Kempes *et al* [4] to include degradation due to antibiotics. The model in Kempes *et al* is a system of coupled differential equations:

$$\frac{dN_r}{dt} = \gamma \frac{r_r}{l_r} N_r - \eta N_r$$
$$\frac{dN_p}{dt} = (1-\gamma) \frac{r_r}{l_p} N_r - \phi N_p$$

Here N_r is the number of ribosomes and N_p is the number of the protein pool. The equations have production terms that represent the role of ribosomes in synthesizing ribosomes and proteins. The production of the ribosomes and proteins is governed by the fraction of mRNA transcripts that are for ribosomal proteins (γ), the rate of translation (r_r) (in base pairs per second), and the average length of ribosomal and protein transcripts, l_r and l_p respectively. Degradation of ribosomes and proteins is represented by η and ϕ, the intrinsic degradation rates associated with ribosomes and proteins. Together the production and degradation terms give the growth rates of the ribosome and protein pools. When modeling ribosome targeting antibiotics we include degradation rates adding another degradation term, kAR, where k is a kinetic rate constant and A is the antibiotic concentration. The

modified degradation rate is then $\eta(A) = \eta + kA$, and

$$\frac{dN_r}{dt} = \gamma \frac{r_r}{l_r} N_r - (\eta + kA) N_r = \gamma \frac{r_r}{l_r} N_r - \eta(A) N_r \tag{1}$$

$$\frac{dN_p}{dt} = (1-\gamma) \frac{r_r}{l_p} N_r - \phi N_p \tag{2}$$

By solving this system analytically and stipulating that ribosomes and proteins must be doubled by the time of division, as done in Kempes *et al* and as suggested by Monod [4, 12], we find the minimum $\gamma(t_d, A)$ and initial number of ribosomes $N_{r,0}(t_d, A)$ for a fixed antibiotic concentration A, initial number of proteins, $N_{p,0}$, and time of division t_d:

$$\gamma(t_d, A) \geq \frac{l_r}{r_r} \big(\frac{\ln 2}{t'_d} + \eta(A) \big) \tag{3}$$

$$N_{r,0}(t_d, A) \geq \frac{l_p (l_r(\phi - \eta(A)) + \gamma r_r)(2 - e^{-t_d \phi})}{l_r(\gamma - 1) r_r \big(e^{-t_d \phi} - e^{t_d (\frac{\gamma r_r}{l_r} - \eta(A))} \big)} N_{p,0} \tag{4}$$

Ribosomal allocation has been shown to vary under different environmental conditions and has been linked to growth rates and cell size *Escherichia coli* [17, 18]. We model the optimal cellular response to antibiotics under the assumption that γ, which represents the allocation of ribosomal resources, is changed in response to the environment. This framework allows us to understand the minimum requirements for cell division, which we use in the following section to model the optimal cellular response in terms of the cell's energy budget and resource allocation.

2.1.2 Energy Budget, Growth Rates, and Antibiotic Stress Response

Cells must split their resources between growth and maintenance. As the antibiotic concentration increases the energy that the cell allocates to maintenance does also. We use the

calculations of the optimal γ and $N_{r,0}$ detailed in the previous section to calculate the change in maintenance cost, and tie this to changes in the doubling time of the cell. Kempes *et al* [15] model the growth rate of the cell using an energy budget which splits cellular resources into maintenance and growth;

$$\frac{dV}{dt} = \frac{B_0}{E_v}V^{\alpha} - \frac{B_v}{E_v}V \tag{5}$$

where B_0 is the parameter for size-normalized metabolism, α describes how quickly metabolism changes with total cell volume (approximated to be 1.43 in prokaryotes), $B_v(\mathrm{W\ m^{-3}})$ is the metabolic expenditure to support an existing unit of cell volume, $E_v(\mathrm{Jm^{-}3})$ is the metabolic energy needed to synthesize a new unit of biomass; $V(\mathrm{m^3})$ is cell volume, $\frac{dV}{dt}$ is the growth rate. The time of division obtained by solving Eq. 5 is

$$t_d = \frac{1 - \frac{b}{a}V_0^{1-\alpha}}{b(1-\alpha)\left[1 - \frac{b}{a}(\varepsilon V_0)^{1-\alpha}\right]} \tag{6}$$

To model changes in growth rate under antibiotic stress, we can recalculate the per volume per second metabolic expenditure, B_v, by incorporating the changes in energy expenditure due to changes in the proportion of ribosomal transcripts $\gamma(t, A)$ and the initial number of ribosomes $N_{r,0}(t, A)$ based on Equations 3 and 4. To do this we first calculate lifetime energy expenditure without antibiotics from B_v, and the energy required to produce proteins and ribosomes over the lifetime of the cell with and without antibiotic stress.

$$C_{tot}(t, 0) = B_v t\overline{V} \tag{7}$$

$$C_r(t, A) = \beta_r\left(\int_0^t \gamma(A)\frac{r_r}{l_r}Rdt - N_{r,0}(t, A)\right) \tag{8}$$

$$C_p(t, A) = \beta_p\left(\int_0^t (1-\gamma(A))\frac{r_r}{l_p}Rdt - N_{p,0}\right) \tag{9}$$

where $C_{tot}(t,0)$ is the lifetime energy spent by the cell, and β_r and β_p are the energetic costs of producing a single ribosome and single protein. We calculate the lifetime energy spent on maintenance under antibiotic stress, $C_{tot}(t,A)$, by adding the energetic cost of ribosomes and proteins under antibiotic stress and subtracting the cost without antibiotics from $C_{tot}(t,0)$. The modified value of the per second per volume metabolic expenditure, $B_v(t,A)$ is then obtained by dividing by time of division and mean volume.

$$C_{tot}(t,A) = C_{tot}(t,0) + C_r(t,A) + C_p(t,A) - C_r(t,0) - C_p(t,0) \tag{10}$$

$$B_v(t,A) = \frac{C_{tot}(t,A)}{t\overline{V}} \tag{11}$$

It should be noted that this calculation of $B_v(t,A)$ is based on the cell optimizing its processes for a given time of division t, but this new value of B_v is then used in Eq. 5 to calculate a time of division.

2.1.3 Calculation of Optimal Time of Division

The modeling framework shown in Equations 3 - 11 represents a bacterial cell optimizing its metabolic processes, in particular its allocation of ribosomal resources, to a predetermined antibiotic concentration and time of division. This "macro-molecular" time of division (t_{mol}) is arbitrarily chosen. The models result in an "energetic" time of division ($t_{energetic}$) by substituting the metabolic expenditure $B_v(t_{mol},A)$ into Eq. 5. The energetically optimal t_{mol} for the cell to respond to is t_{mol} such that $t_{mol} = t_{energetic}$. This is because t_{mol} is the time at which the ribosome and protein pool are doubled, and $t_{energetic}$ is the time at which the cell actually divides. If $t_{energetic} < t_{mol}$, then the cell will have divided before the ribosome and protein pools have been doubled, and if $t_{energetic} > t_{mol}$ then the ribosome and protein pools will be more than double their original sizes, which is sub-optimal because this requires the

cell to spend more energy on ribosome and protein production than required. In both cases, the macro-molecular composition of the cell will drift across generations, which homeostasis, which we assume to be required even under antibiotic stress. Calculating the optimal or "self-consistent" time of division is not possible analytically, so we calculate it numerically using the bisection method (Figure 5, Section 4.1.1) . This allows us to calculate the minimum time of division under model assumptions at any antibiotic concentration, which can then be used in the generation of dose-response curves.

2.1.4 Antibiotic Diffusion Across Cell Membrane

While theory presented thus far has been framed in terms of the antibiotic concentration inside the cell, our over-arching goal is to compare our theoretical results with our experimental results. We control the antibiotic concentration external to the cell in our experimental work, and therefore model the movement of the antibiotic across the cellular envelope. We can match the internal dynamics of the antibiotic effects with the outside concentration of the antibiotic by considering the diffusive flux of antibiotics to the cell. This can be easily approximated by considering an internally well-mixed spherical cell with an internal steady-state concentration of antibiotic, where we then match the steady-state flux to the cell with the internal consumption. The steady-state diffusive flux can be found by considering the diffusion equation under spherical symmetry:

$$\frac{1}{r^2}\frac{\partial}{\partial r}\left(r^2\frac{\partial A}{\partial r}\right) = 0. \tag{12}$$

To separate the internal reaction dynamics from the flux dynamics we impose a boundary condition at the surface of the cell that is equivalent to the well-mixed internal concentration: $A = A_c$ for $r = r_c$. The other boundary condition is that far from the cell the antibiotic is held to the known fluid concentration: $A = A_f$ for $r = \infty$. Taken together this gives the

concentration field of the antibiotic outside of the cell as

$$A = A_f - \frac{(A_f - A_c)\, r_c}{r}, \tag{13}$$

from which the total flux at the surface is given by

$$F = 4\pi r_c^2 D \frac{\partial A}{\partial r} = 4\pi D r_c \,(A_f - A_c)\,. \tag{14}$$

Now we can solve for the total internal reaction separately and find the A_c that matches external flux to internal consumption.

In the case of an antibiotic that targets ribosomes, the internal consumption is approximated by $kA_c\overline{N_r}$, where $\overline{N_r}$, the number of ribosomes averaged over the cell's lifetime, is dependent on A_c. Therefore the effective internal concentration is related to the external concentration by $A_f = \left(\frac{kN_r r_c^2}{4\pi D} + 1\right)A_c$, where N_r is determined by the internal antibiotic concentration.

2.1.5 Generation of Dose Response Curve

We now use the previous theoretical work on how the time of division and external antibiotic concentration can be determined for a cell with a given internal antibiotic concentration and cell volume to produce dose-response curves that are comparable to experimental measurements. To do this we calculate the number of cells after 24 hours for a range of antibiotic concentrations using a logistic growth model for the number of cells (N)

$$\frac{dN}{dt} = \frac{\ln 2}{t}\left(\frac{K - N}{K}\right)N \tag{15}$$

where the carrying capacity K and the initial number of cells N_0 correspond to values determined from experimentation.

2.2 Incorporation of Cell Volume in Dose-Response Model for Ribosome-Targeting Antibiotics

Because the percentage volume of components that are targeted by antibiotics shift with cell size [4], we expect that antibiotic susceptibility will shift due to cell volume effects. In the following sections we incorporate these shifts in composition into the model outlined in the previous section to make predictions of size dependencies in inhibitory antibiotic concentrations.

2.2.1 Shifts in Cellular Composition with Cell Size

The relationship between cell volume and several components can be approximated by power-law relationships (of the form $V_{component} \propto V_{cell}^{\beta}$) [4]. Additionally, growth rate is dependent on cell volume due to cell size dependencies in energy budgets modeled in Eq. 5. The volume of other components (ribosomes, tRNA, and mRNA) is then calculated as the minimum volume required for all of the cellular components to double by the time of division that is derived from the size dependent time of division. This calculation is equivalent to the calculations in Eq. 3 - 4, where the antibiotic concentration is 0 and γ and $N_{r,0}$ are calculated with t_d and $N_{p,0}$ specified by cell size. The relationships between component volume and cell volume is specified in the Table below.

Component	Relationship with Cell Volume	Unit
Metabolic Rate (B)	$B_0 V_c^{\beta_B}$	W
Growth Rate (μ)	$\frac{(B_v/E_v)(1-\beta_B)\ln\epsilon}{\ln[1-(B_v/B_0)(V_c d_c)^{1-\beta_B}]-\ln[1-\epsilon^{1-\beta_B}(B_v/B_0)](V_c d_c)^{1-\beta_B}]}$	s^{-1}
Protein Volume (V_P)	$P_0 V_c^{\beta_P}$	m^3
Ribosome Volume (V_R)	$\frac{\bar{l}_p N_p(\phi/\eta+1)}{r_r/\mu-\bar{l}_r(\eta/\mu+1)}$	m^3
tRNA (V_{tRNA})	$\overline{v}_{tRNA}\overline{n}_{tRNA}N_R$	m^3
mRNA (V_{mRNA})	$\overline{v}_{mRNA}\overline{n}_{mRNA}N_R$	m^3
Cellular Envelope (V_{env})	$\big(V_c-\frac{4}{3}\pi\big[\big(\frac{3V_c}{4\pi}\big)^{1/3}-r_{env}\big]^3\big)(1\text{-}\overline{p}_P)$	m^3

Table 1: Relationships between component volume and cell volume from derivations in Kempes *et al.* Parameters are defined with their values in Table 2

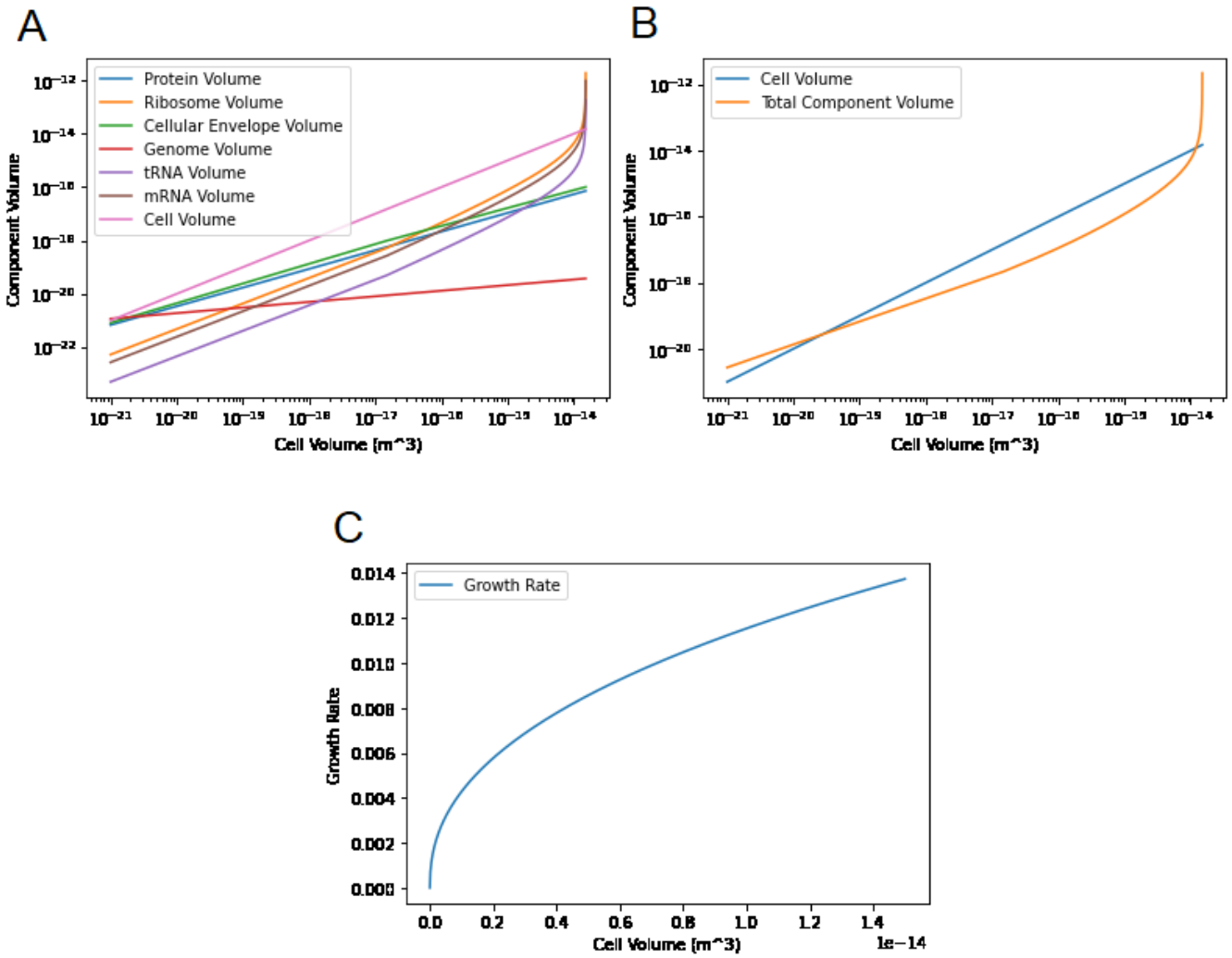

Figure 2: **Shifts in cellular composition with cell volume** Previous results from Kempes *et al*, (A) Log-log plot of cell volume and components volume. Ribosome, protein mRNA, tRNA, genome, and cellular envelope volume all shift with cell size. (B) Required dry volume (orange) compared with cell volume (blue). Lower and upper bounds on cell size are created by the total required dry volume exceeding the cell volume, where the two curves intersect. (C) Growth rate, calculated as $\mu = \frac{ln2}{t_d}$ where t_d is doubling time increases non-linearly with cell-size.

2.2.2 Incorporation of Cell Size Dependencies into Dose-Response Model

The dose response model outlined in Section 3.1 calculates the optimal response to a specified antibiotic concentration by connecting the molecular dynamics of the cell the energetic costs, and finds the time of division under this response. In the case of the ribosome-targeting antibiotic the functioning of ribosome is essential for growing and maintaining the standing pool of proteins. We assume that there are pre-defined requirements for the number (or volume) of the protein pool that must be met by the ribosome pool and adjustments in resource distribution (modeled here by γ, the fraction of ribosomal transcripts). We incorporate cell size effects in the ribosome model through the size dependence on the protein pool, as protein number and volume ($N_{p,0}$ in Eq. 4) is modeled to have a power-law relationship with cell volume.

2.2.3 Volumetric Constraints at Extreme Cell Sizes

In addition to the cell-size dependence due to energetic factors considered thus far, the flexibility in cellular composition can be limited by cell size. In particular, we note that it is a biological impossibility for the total volume of required components to exceed cell volume, but the dry volume fraction in cells that are responding to ribosome-targeting antibiotics increases sharply in our model. This increase occurs because (i) the number of ribosomes is up-regulated to compensate for degradation due to the antibiotic, and (ii) the ribosome-antibiotic complexes are assumed to degrade at the same rate as ribosomes or slower. Therefore the required dry volume can exceed the cell volume at antibiotic concentrations that are calculated to be sub-lethal from the energy-based model in Section 2.1. This is particularly limiting at extremely large and small cell sizes, at which the dry volume fraction is high even without antibiotic stress (Figure 2B). The volume limiting antibiotic concentration is then defined as the antibiotic concentration at which the the required dry volume fraction is equal to the cell volume. The mean dry volume fraction $\overline{V}_{component}(V_c, A)$

is a function of both antibiotic concentration and cell volume, V_c.

$$\overline{V}_{component}(A, V_c) = \frac{\int_0^{t_d} \left(v_r N_r(A,t) + v_p N_p(A,t) + V_{t_RNA}(A,t) + V_{mRNA}(A,t)\right) dt}{t_d} + V_{env} \tag{16}$$

where the number (and volume) of mRNA and tRNA transcripts is proportional to the number of ribosomes (Table 2.2.1), and the number of ribosomes and proteins are defined by the solutions to Eq. 1 and 2, with γ and $N_{r,0}$ given by Eq. 3 and Eq. 4, and $N_{p,0}$ given by the size-dependent power law relationship defined above. We then use the bisection method to find the numerical solution for A such that $V_{component} = V_c$, which gives us the volume-limiting minimum inhibitory concentration, MIC_v. The overall predicted inhibitory concentration is the minimum of the MIC_v found here and the energetically limiting concentration predicted based on Section 2.1.

	Parameter	Value	Unit
V	Cell Volume	(varies between $10^{-21} - 10^{-15}$)	m^{-3}
η	Intrinsic degradation rate for ribosomes	6.19×10^{-5}	s^{-1}
ϕ	Intrinsic degradation rate for proteins	6.19×10^{-5}	s^{-1}
γ	Proportion of ribosomal transcripts	(derived above)	
k	Kinetic rate constant	free parameter	$M^{-1}s^{-1}$
t_d	Time of division	(derived above)	s
α	Bacterial growth scaling exponent	1.43	Unitless
B_0	Parameter for size-normalized metabolism	2.31×10^{12}	W $m^{-(3(\alpha-1))}$
B_v	Metabolic expenditure to support an existing unit of cell volume	1.22×10^{3}	Wm^{-3}
E_v	Metabolic expenditure to synthesize an existing unit of cell volume	2.21×10^{8}	Jm^{-3}
β_r	Average energetic cost of producing a ribosome	2.70×10^{-15}	J per protein
β_p	Average energetic cost of producing a protein	9.79×10^{-17}	J per protein
d_c	Cell density	1.1×10^{6}	gm^{-3}
v_r	Volume of single ribosome	3.04×10^{-24}	m^3
v_{mRNA}	Volume of single mRNA	1.43×10^{-21}	m^3
v_{tRNA}	Volume of single tRNA	3.10×10^{-26}	m^3
β_P	Volume scaling exponent for proteins	0.7 ± 0.06	Unitless
P_0	Power law constant for size scaling of proteins	3.42×10^{-7}	$m^{-3\beta_P}$
$\overline{p}_p$	Average proportion of cellular envelope that is occupied by protein (by volume)	0.15	Unitless
K	Carrying Capactiy	6×10^{7}	Number of cells

Table 2: Parameter definitions and values used in theoretical model

3 Methods

3.1 Experimental Methods

3.1.1 Bacterial Species

We chose 12 bacterial species with a range of cell volumes across seven orders of magnitude 10^{-13} to 10^{-19} m^3 (as assessed from the literature - see Table 3). Most species were obtained from ATCC (given website) and inoculated in 6 mL of appropriate media at optimal temper-

atures/conditions (Table 1). Cultures were grown aerobically until they reached stationary phase, between 24-48 hours. Cultures were spun at 3500 rpm 4℃ for 10 minutes, the supernatant was discarded and the pellet was resuspended in 3 mL of 20% glycerol. Permanent stocks were prepared using 2 mL of the 20% glycerol resuspension. The remaining 1mL was distributed into 50 µL aliquots reserved as working stocks. All stocks were stored at -80℃. At the start of each experiment, one 50L aliquot was thawed, inoculated in 2 mL of the appropriate media and incubated at the optimal temperature for 16-22 hours.

Bacterial Species	**Optimal Temperature (°C)**
Bacillus licheniformis	38
Bacillus megaterium	37
Bacillus subtilis	37
Escherichia coli	37
Lactococcus lactis	37
Pseudomonas fluorescens	30
Pseudomonas natriegens	32
Pseudomonas putida	30
Staphylococcus epidermidis	36
Staphylococcus thermophilus	38
Lactobacillus plantarum	37

Table 3: Bacterial Species and Optimal Temperatures

3.1.2 Antibiotics

We chose to use antibiotics from a variety of classes and mechanisms of action (summarized in Table 4) [19–32]. All antibiotic stocks were prepared at 20 mg/mL, with the exception of antibiotics that had a maximum solubility of less than 20 mg/mL. A list of the antibiotics used and information regarding stock concentrations can be found in Table . Antibiotic stocks were prepared by dissolving the powder form into their respective solvents: erythromycin, nalidixic acid and spiramycin were dissolved in ethanol, and spectinomycin, sulfamonomethoxine and trimethoprim were dissolved in 100% DMSO. All other antibi-

otics were dissolved in autoclaved MilliQ water. All antibiotics were purchased from Sigma (St. Louis, MO) with the exception of ciprofloxacin (CPR) which was purchased from MP Biomedicals (Santa Ana, CA).

Antibiotic	**Target Component**	**Target Metabolic Process**
Amikacin	30S Ribosomal Subunit	Protein synthesis
Amoxicillin	Penicillin Binding Proteins	Cell wall synthesis and repair
Ampicillin Sodium Salt	Penicillin Binding Proteins	Cell wall synthesis and repair
Cefoxitin Sodium Salt	Penicillin Binding Proteins	Cell wall synthesis and repair
Chloramphenicol HCl	50S Ribosomal Subunit	Protein synthesis
Ciprofloxacin HCl	DNA Topoisomerase , DNA-gyrase	DNA replication, transcription, and repair
Clindamycin HCl	50S Ribosomal Subunit	Protein synthesis
Doxycycline hyclate	30S Ribosomal Subunit	Protein synthesis
Erythromycin	50S Ribosomal Subunit	Protein synthesis
Fusidic Acid Sodium Salt	EF-G-GDP (Elongation Factor)	Protein synthesis
Gentamycin Sulfate Salt	30S Ribosomal Subunit	Protein synthesis
Levofloxacin	DNA Topoisomerase IV, DNA-gyrase	DNA replication, transcription, and repair
Lomefloxacin HCl	DNA Topoisomerase IV, DNA-gyrase	DNA replication, transcription, and repair
Nalidixic Acid Sodium Salt	DNA-gyrase	Transcription
Oxacillin Sodium Salt	Penicillin Binding Proteins	Cell wall synthesis and repair
Penicillin G Sodium Salt	Penicillin Binding Proteins	Cell wall synthesis and repair
Piperacillin Sodium Salt	Penicillin Binding Proteins	Cell wall synthesis and repair
Rifampicin	RNA Polymerase	RNA synthesis
Spectinomycin HCl	30S Ribosomal Subunit	Protein synthesis
Spiramycin	50S Ribosomal Subunit	Protein synthesis
Streptomycin Sulfate Salt	30S Ribosomal Subunit	Protein synthesis
Sulfamonomethoxine	Folic Acid	Nucleic acid synthesis
Tobramycin Sulfate Salt	50S Ribosomal Subunit	Protein synthesis
Trimethoprim	Dihydrofolic Acid (DHF)	DNA synthesis

Table 4: Summary of antibiotics and corresponding mechanisms of action used for experimental work. Rows with ribosome targeting antibiotics are highlighted.

3.1.3 Temperature Assays

To identify the optimal temperature ranges for each species, we performed initial optimal temperature assays across 10 temperatures ranging from 24℃ - 42℃ in increments of 2℃. Each species was grown over-night, until exponential growth phase was reached. Cultures were diluted in appropriate media to a concentration of 10^3 cells per mL. Using 96-well plate (Fisher, Costar), we aliquoted the 15 species, 1 per column, resulting in 8 replicates per species. The last column contained media only to serve as negative controls. The plates were placed in the Tecan Infinite Pro 2000 plate reader and optical density was read at 500 nm and 600 nm every 20 minutes for 24 hours. This procedure was repeated for each of the 10 temperatures. Growth rates and carrying capacity for each species were calculated at each temperature and determined the temperatures at which dose-response assays were conducted (Table 3, Figure 3). Dose-response assays were conducted at the optimal temperatures for all antibiotics. Additionally, for the eight antibiotics (CHL, CPR, ERY, FUS, GEN, LEV, STR, TOB) that were expected to interact strongly with temperature (Cruz-Loya et al.), two additional dose response assays were conducted at temperatures above and below the optimal.

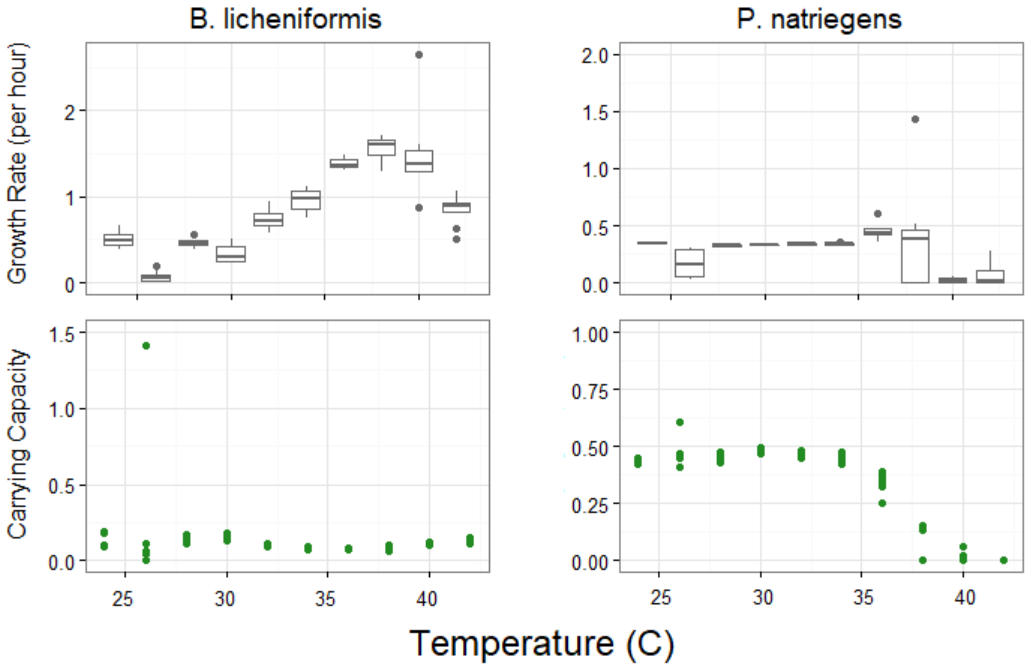

Figure 3: **Temperature response curves for *B. licheniformis* and *P. natriegens*** Temperature curves were used to estimate optimal temperatures for experimental work by fitting a logistic growth model to estimate carrying capacity and growth rates, and dose-response curves were measured at optial temperatures for each species.

3.1.4 EC95 and MIC Measurements

To determine MIC for each of 24 antibiotics across all 12 species, we used 96-well plates. Each plate had a single bacterial species and 8 antibiotics (one per row, diluted across columns 1-11). Column 12 served as the control column, with the positive controls (media and bacteria, with no antibiotic) in the top four wells and negative controls (media alone) in the bottom four wells. The plates were prepared by adding 100L of media plus antibiotic and 100L of diluted overnight culture (105 cells/mL). Plates were incubated for 24 hours at each measured temperature(s) and growth was determined using optical density (OD600).

Round 1: An 11-step 2-fold dilution for each antibiotic-species combination was prepared. Starting at 400µg/mL in column 1, we performed a 2-fold serial dilution of the antibiotics in

media through column 11. Column 12 contained the positive and negative controls. Finally, 100L of overnight culture ($\sim 10^3$ cells/mL) was aliquoted across the plate (except negative control) to obtain a final volume of 200L per well.

Round 2: An 11-step linear dilution for each antibiotic was set up, with the range of antibiotic concentrations expected to include the MIC based on Round 1 respectively. This step varied by species and antibiotics and was performed in triplicate. Liquid MIC is defined as the lowest concentration at which no growth was observed, and EC95 was defined as the interpolated value at which 95% growth was inhibited.

3.1.5 Microscopy to Estimate Bacterial Cell Sizes

We used microscopy to measure bacterial cell sizes and estimate bacterial cell volumes. Images were acquired on a Zeiss AxioImager M1 fluorescence microscope with a 100X Plan-Apochromat objective using the MetaMorph software (Molecular Devices, Sunnyvale, CA). Wet mounts of approximately 5 µL of overnight culture was prepared on glass slides. Images of each species were taken and 10 bacterial cells were measured per species. In order to get an accurate sample of the population, we measured both actively dividing and single cells for each species. We used the LineScan tool in the MetaMorph offline software and took three measurements; cell base length (B_L), cell base height (B_H) and tip radius (T_R) (Figure 4). If the cells were cocci (ex. *S. epidermidis* and *L. lactis*), we measured the cell diameter (d). Initial measurements from the images were measured in pixels, and later converted to µm (1 pixel = 0.1 µm). Cell volumes (V_c) were calculated based off of the initial measurements described below.

To calculate total cell volume for bacilli, the volume of the base (V_B) was calculated by $V_B = \pi B_L B_H$, the volume of the tips (V_T) were calculated by $V_T = \frac{4}{3}\pi T_R^3$, and V_c was estimated as $V_B + V_T$. To calculate total cell volume for cocci we used $V_c = \frac{1}{6}\pi d^3$.

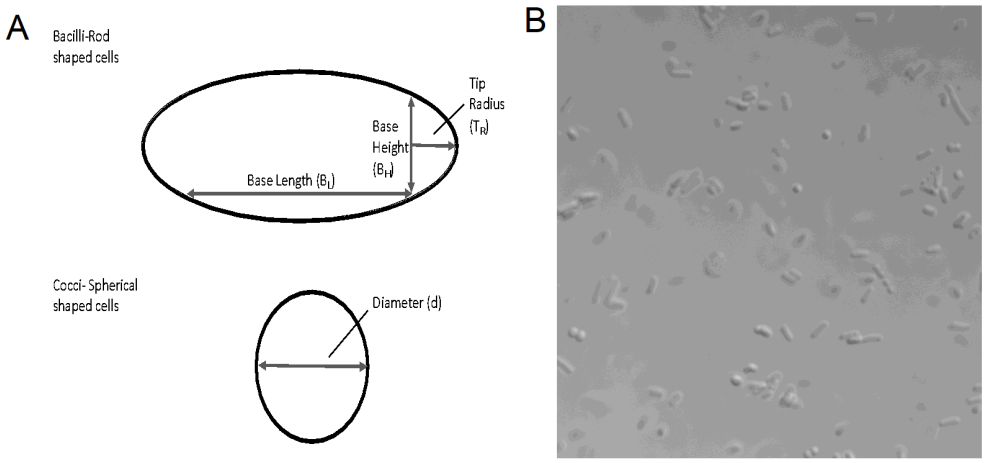

Figure 4: **Measuring cell Size with microscopy**(A) Schematic of the measurements taken to estimate bacterial cell size. The measurements that were taken for bacilli (rod-shaped) cells were the base length, base height, and the tip radius. The tip radius measurement begins at the base height measurement and spans to the end of the cell tip. The only measurement taken for spherical cells was the diameter. These measurements were used to calculate total cell area and volume. (B) Example image of *Staphylococcus epidermidis* culture

3.2 Fitting Dose-Response Data

We fit normalize experimental data by the growth in the positive control, where the bacteria is grown with no antibiotic. We then fit an inverse Hill function to the data with the form

$$g(A) = 1 - \frac{A^n}{EC50^n + A^n} \tag{17}$$

Here A is antibiotic concentration, and $g(A)$ is the growth after 24 hours at antibiotic concentration A. EC50 is the concentration at which the growth is at half of the maximum growth, and n is a parameter that controls the sharpness of the curve. We fit the data using non-linear least squares.

3.3 Fitting Model to Dose-Response Data

The dose-response curves generated from our model are similar in shape to the inverse Hill function described above, and we use free parameters k and D to fit our model to the curve described above. We define a cost-function by calculating the squared horizontal distance between the two curves at 8 points.

The squared horizontal distance between two dose-response curves with parameters $EC50_1$, n_1 and $EC50_2$ and n_2 is defined for a fixed value of g:

$$d_g^2(EC50_1, n_1, EC50_2, n_2) = \left(EC50_1 \left(\frac{1-g}{g} \right)^{\frac{1}{n_1}} - EC50_2 \left(\frac{1-g}{g} \right)^{\frac{1}{n_2}} \right)^2 \tag{18}$$

The cost function for the two curves is then defined as

$$\sum_{g_i} d_{g_i}^2(EC50_1, n_1, EC50_2, n_2) \tag{19}$$

where $g_i \in \{0.1, 0.2, 0.3, 0.4, 0.5, 0.6, 0.7, 0.8, 0.9\}$. We then minimize this cost function over k for a fixed value of D or vice versa to fit the theoretical model to the curve derived from data.

4 Results

We tie together theoretical predictions on the effects of cell size on antibiotic susceptibility with experimental observations. The theoretical model presented in Section 2.1 can be used to generate dose-response curves that are qualitatively similar to our data, and we are able to fit dose-response curves using antibiotic-specific free parameters. Size-dependent shifts in metabolic processes and cellular composition can then be incorporated to make cross-species predictions of antibiotic susceptibility. We identify multiple fundamental constraints on cells - the energy and the volume available to the cell. We predict two inhibitory concentra-

tions corresponding to these constraints - an "energy-limiting" concentration, at which the growth is inhibited to 5% due to limitations in the cell's ability to divide (Section 2.1), and a "volume-limiting" concentration, at which the required dry volume of components and target-antibiotic complexes exceeds the cell volume (Section 2.2.3).

For ribosome and cell-wall targeting antibiotics we observe experimentally that mid-sized cells are the least susceptible, suggesting that there are complex trade-offs related to cell size that affect antibiotic susceptibility. We build on the result from Kempes *et al* that dry-volume fraction is lowest in mid-sized cells. This suggests that cells that are extremely large or small are constrained by limitations on space within the cell in addition to molecular dynamics and energetic constraints, leading to "energy-limited" and "volume-limited" regimes in cell size, which could explain the experimental trends that we observe.

4.1 Theoretical Dose-Response Model

4.1.1 Dose-Response Curves can be Generated From Theoretical Model

We detail a model connecting molecular dynamics, resource redistribution, and the overall energetics and growth of the cell in Section 2.1, which we can use to generate dose response curves. This model integrates diffusion of the antibiotic into the cell membrane, molecular dynamics, and overall energetics of the cell.

We first present results on the relationship between the internal antibiotic concentration, time of divsion, and growth, based on the model outlined in Section 2.1. The cell optimizes the proportion of ribosomal transcripts (γ) and the number of initial ribosomes in the cell ($N_{r,0}$), so that the protein pool – which is assumed to be fixed under antibiotic stress – and the ribosome pool are doubled (Eqs. 3 and 4). Resource distribution thorugh γ and $N_{r,0}$ is optimized based on a specific "macromolecular" time of division (t_{mol}), and results in increases in the metabolic expenditure (B_v). An increase in B_v then result in an increase in the energetic (actual) time of division of the cell ($t_{energetic}$).

We find the intersection of t_{mol} and $t_{energetic}$, the time of division resulting from optimizing macromolecular parameters based on t_{mol}, to give the minimum time of division (Figure 5A). This is the miimum time of division because when $t_{mol} > t_{energetic}$ the cell divides before all of the components are doubled, and when $t_{mol} < t_{energetic}$ the ribosome and protein pools are more than double their initial size, which increases the metabolic expenditure and results in a longer time to divide than necessary. In both cases the cellular composition will shift across generations. Figure 5A shows the intersection of the macromolecular time of division that is optimized on (blue) with the resulting "energetic" time of division at low (orange) and high (red) internal antibiotic concentrations. The orange and red points on Figures 5B and C correspond to the two antibiotic concentrations shown in Figure 5A. We note that the optimal time of division increases with internal antibiotic concentration (Figure 5B), which results in fewer cells after 24 hours under a logistic growth model (Figure 5C). This is particularly useful because we approximate the number of cells after 24 hours in our experimental system.

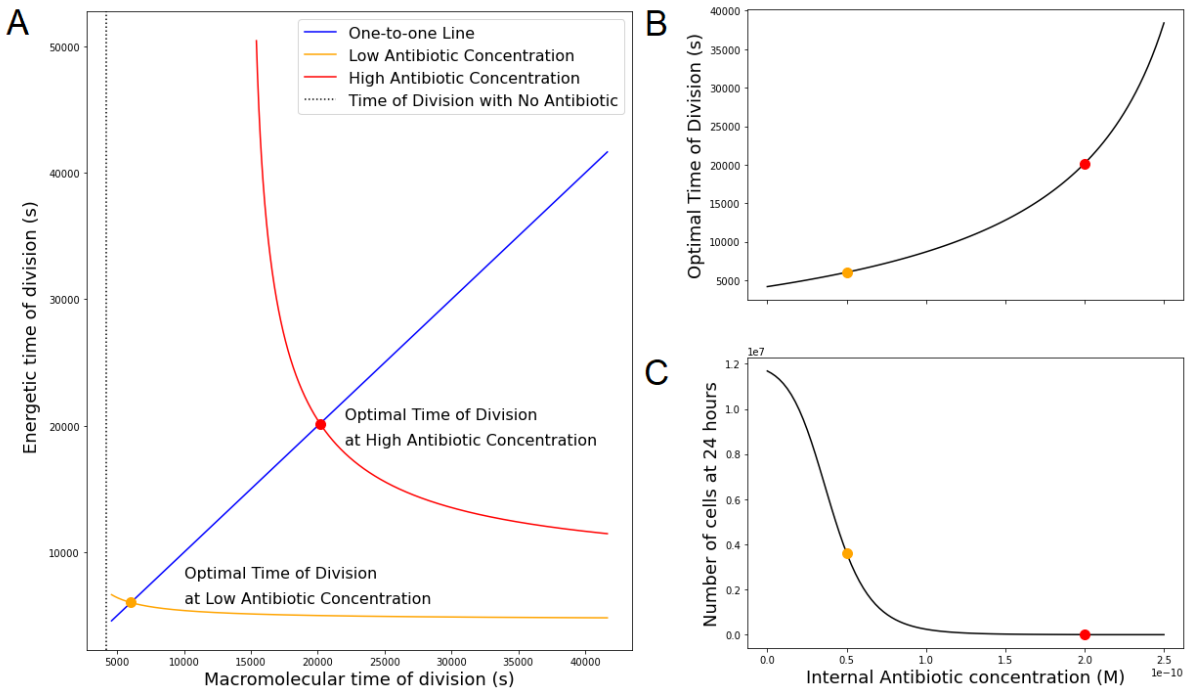

Figure 5: **Generation of dose-response curves** (A) Plot showing the intersection of the energetic time of division resulting from the macro-molecular time of division at low (orange) and high (red) antibiotic concentrations, (B) Optimal time of division increases with internal antibiotic concentration, and (C) Dose-response curve resulting from the model, with number of cells after 24 hours decreasing with antibiotic concentration.

The results thus far have focused on the effect of the internal antibiotic concentration on the growth of the cell. Modeling the diffusion of the antibiotic into the cell allows us to compare our experimental results directly to theoretical predictions, as external antibiotic concentration is the free parameter that we control in our experimental work. The detailed model presented in Section 2.1.4 finds the steady-state internal antibiotic concentration by incorporating the flux created by the binding of the antibiotic to ribosomes and the surface area of the cell. We find that internal concentration increases non-linearly with external antibiotic concentration (red curve in Figure 6), and that the dose-response curves incor-

porating diffusion produces a qualitatively similar curve (green in Figure 6) to the curve produced just using internal antibiotic concentration (Figure 5C). The next results are presented incorporating diffusion.

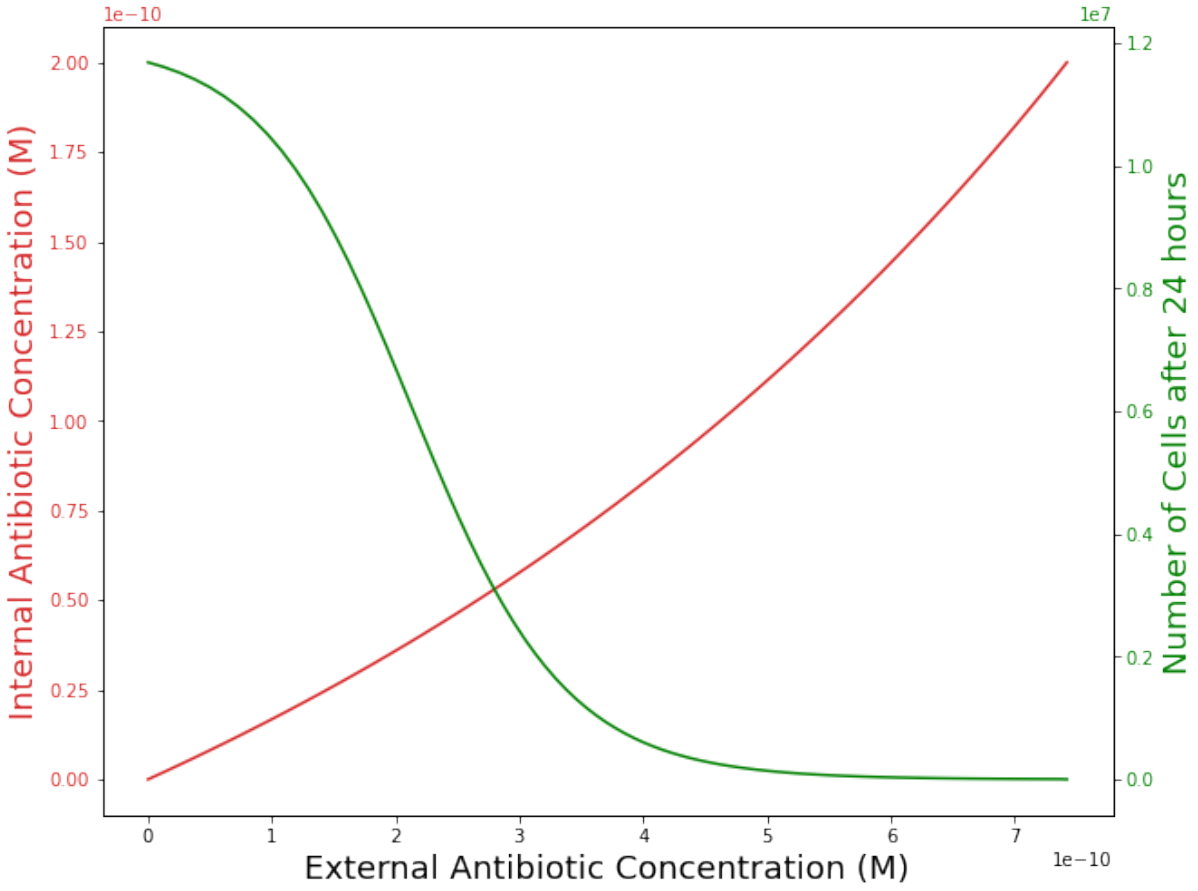

Figure 6: **Effects of diffusion on molecular dynamics** (A) Relationship between external and internal antibiotic concentration of a cell, which depends on the surface area of cell membrane and the concentration gradient created by the antibiotic-ribosome dynamics within the cell, and (B) Dose-response curve incorporating diffusion of antibiotic into the cell

In addition to the the results based on changes in the cellular energy budget due to the molecular dynamics, we consider the space limitations imposed due to the size of the cell. In Section 2.2.3, we consider the fact that the antibiotic-ribosome complexes increase

the dry volume of the cell, which could create an additional constraint because the total required volume of cellular components cannot exceed cell volume. We calculate the total required dry volume fraction at several antibiotic concentrations, and we note that the total required dry volume of the cell, which includes the volume of ribosomes, proteins, mRNA, tRNA, the cellular envelope, genome, and the antibiotic-ribosomes complexes, increases with antibiotic concentration. Figure 7 shows that for a cell the size of *Escherichia coli* the required dry volume fraction increases (blue) beyond the volume of the cell at high antibiotic concentrations. This is largely driven by increased levels of ribosome-antibiotic complexes at high antibiotic concentrations (orange). This model allows us to predict a "volume-limiting" concentration at which the required dry volume increases to the volume of the cell, in addition to the inhibitory concentrations shown previously. The overall inhibitory concentration predicted for a cell is then the minimum of the volume-limiting and energy-limiting concentrations.

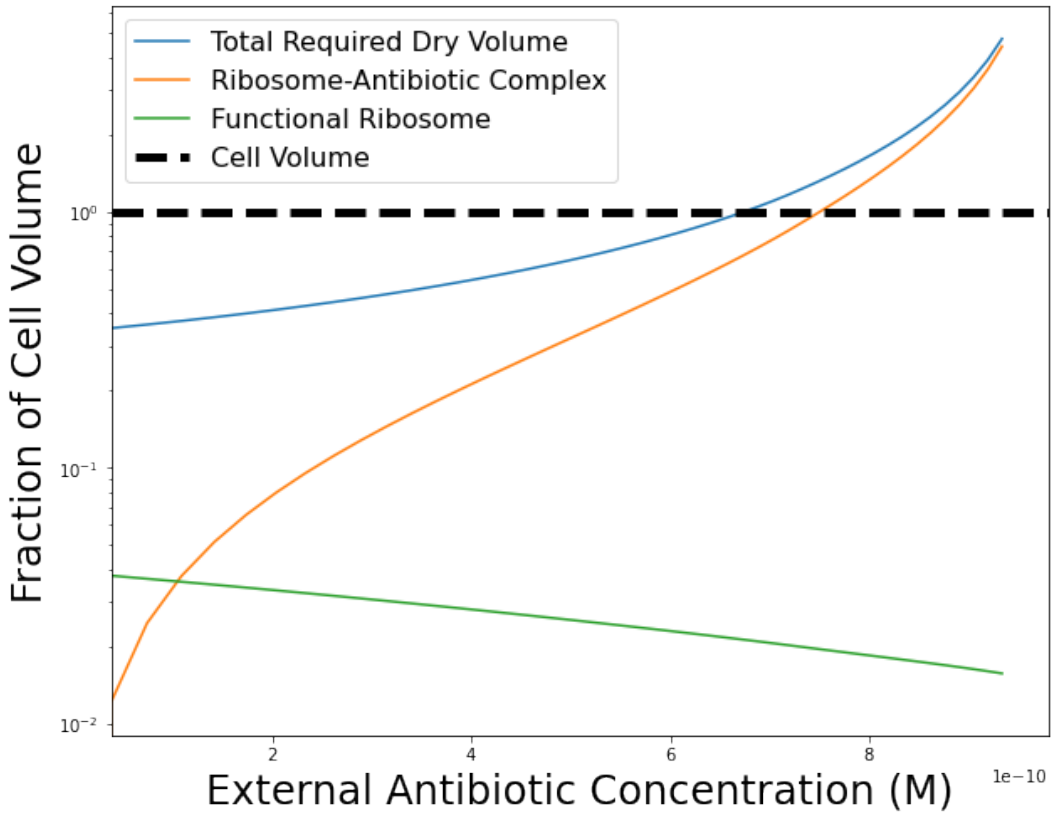

Figure 7: **Increases in required dry volume under antibiotic stress can inhibit growth** Cellular composition based on optimal energetic response shifts with antibiotic concentration. The volume of antibiotic-ribosome complexes increase in volume with antibiotic concentration, increasing the total dry volume of the cell beyond the cell volume, which is a biological impossibility. The upper limit on the dry volume that a cell can tolerate is likely much less than 100%.

4.1.2 Resource Redistribution Under Antibiotic Stress

In addition to generating dose-response curves, we are able to gain insights into the optimal resource redistribution under antibiotic stress. Under our model assumptions the cell responds to antibiotic stress by modifying the partitioning of mRNA transcripts between transcripts for ribosomal and non-ribosomal proteins, and by changing the initial number of

ribosomes. These two changes result in a shift in the metabolic expenditure for maintaining the cell, which modifies the time of division. Figure 8C shows that increasing antibiotic concentration results in increases in metabolic expenditure, B_v, which drives a decrease in growth rate (Eq. 5), and therefore an increase in time of division (Eq. 6). This results in a decrease in the number of cells after 24 hours (Figure 5C, 6).

Resource distribution is modeled in terms of the proportion of ribosomal transcripts and minimum number of ribosomes that minimized time of division for any given antibiotic concentration. Interestingly, we find that while the proportion of ribosomal transcripts, γ, increases, the initial number of ribosomes is down-regulated. The decrease in the number of initial ribosomes ($N_{r,0}$) also decreases the number of ribosomes that the cell must have in order to divide by the time of division, which is $2N_{r,0}$, as the cell needs to double the ribosomal pool so that the cellular composition is maintained across generations. This decrease in the total number of ribosomes required at the end of the cell cycle combined with the increase in time of division can compensate for the higher ribosome production that is required by additional degradation due to antibiotics.

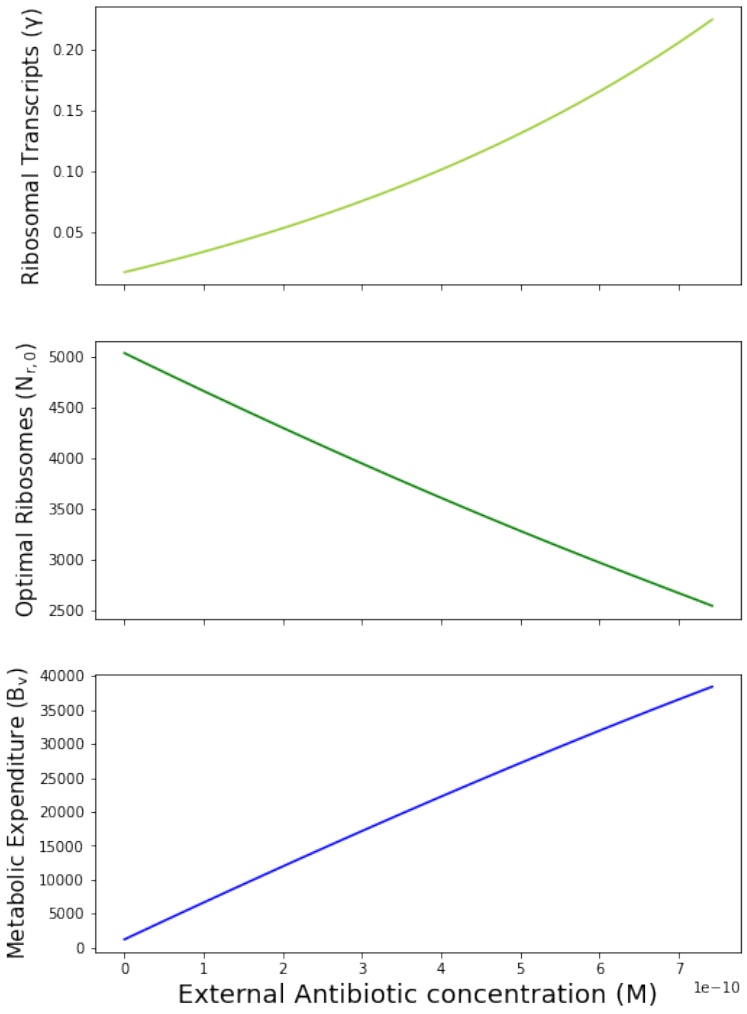

Figure 8: **Resource redistribution and energetic costs under antibiotic stress** (A) The proportions of ribosomal transcripts, γ, increases under antibiotic stress, as ribosomal resources are reallocated towards producing more ribosomes in response to increases degradation due to antibiotics. (B) The initial number of ribosomes decreases under antibiotic stress, which minimizes energy spent on producing ribosomes that are degrading faster due to antibiotics. (C) The metabolic expenditure per unit time and volume increases under antibiotic stress, resulting in slower growth rates.

4.1.3 Theoretical Models can be Fit to Dose-Response Data

The theoretical results presented thus far have shown that dose-response curves that are qualitatively similar to dose-response data measured experimentally can be generated for fixed values of the rate constant, k (detailed in Eq.1), the rate at which antibiotic binds to ribosomes, and the diffusion constant D, the rate at which the antibiotic diffuses across the cellular membrane. Because these kinetic parameters are difficult to measure precisely and could depend on antibiotic and species specific traits, literature values vary widely [33]. We therefore leave these as free parameters that can be used to fit the model to data. Figure 9A and 9B shows that dose-response curves are sensitive to both k and D respectively, and that varying these parameters allows us to shift the dose-response curve be several orders of magnitude. We note that as D is increased the curves converge, indicating an asymptote for minimum inhibitory concentrations as D increases. We fit the curves shown in 9A and 9B as described in Section 3.2, to estimate the $EC50$ and n parameters from these curves, as shown in Fig. 9C and 9D. We note that as D increases the sharpness of the curve (n) and the $EC50$ value decrease, whereas when k increases the $EC50$ parameter decreases but the sharpness of the curve (n) increases. We note that n appears to have upper and lower bounds when both k and D are changed, indicating that there might be a limiting range of sharpness in the curves generated from the theoretical model. The trade-offs between changing cell volume, k, and D are still unclear, and understanding this is an avenue for future work.

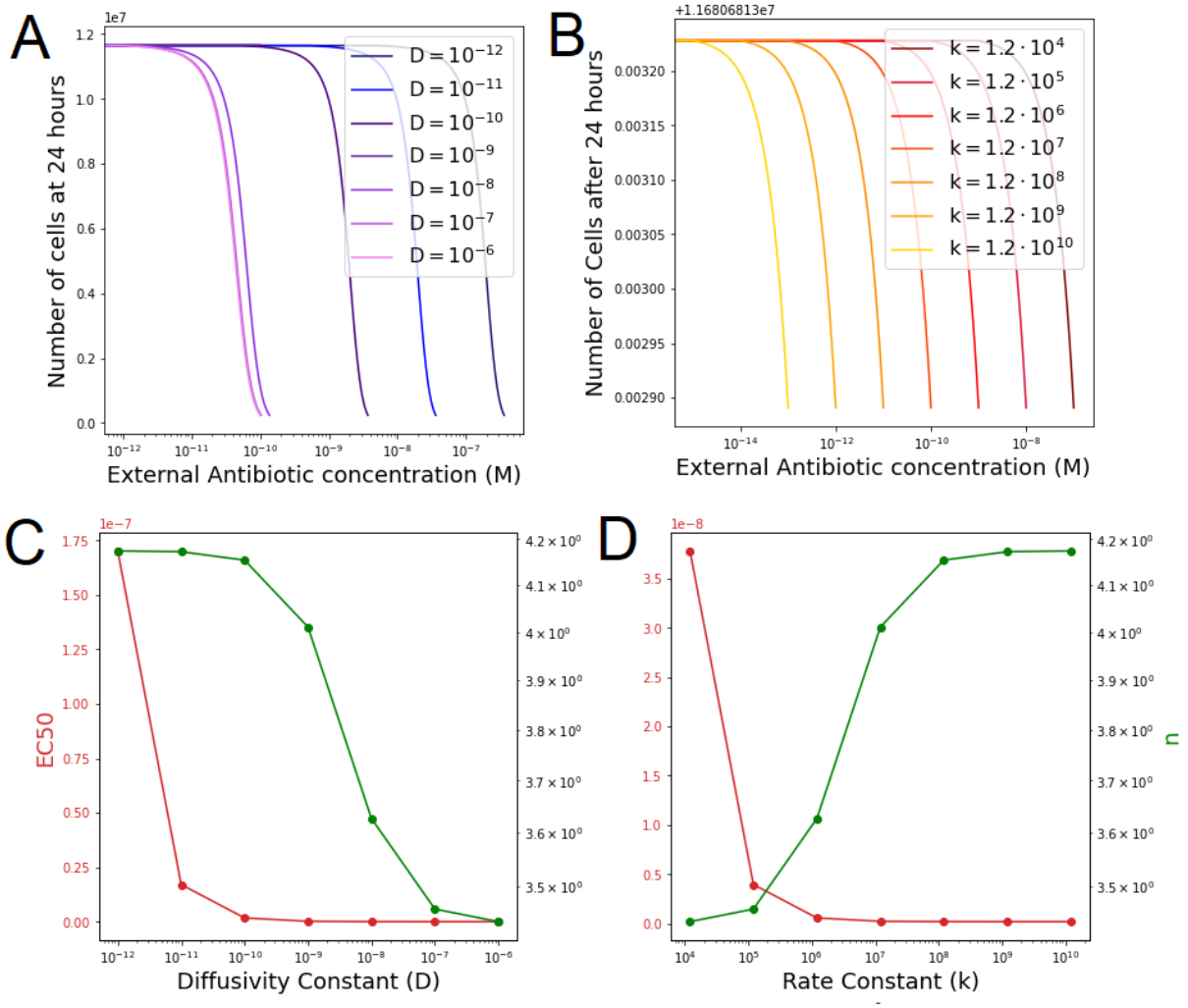

Figure 9: **Model sensitivity to free parameters** (A) Model sensitivity the diffusion constant, D and (B) the rate constant k. (C)Estimated $EC50$ (inhibitory concentration that reduces growth by 50%) and n (parameter indicating sharpness of the dose response curve) from dose response curves generated by the theoretical model for a range of (C) values of k and D (Panel D). Panels A and B show that we are able to shift the dose response curve by several orders of magnitude by changing the values of k and D, and Panels C and D show that $EC50$ decreases exponentially with both K and D, whereas the sharpness of the curve decreases with D and increases with k. The sharpness parameter n appears to have an upper bound of 1.75 and 3.75 with D and k respectively.

For fixed values of D and cell volume we are able to fit our theoretical model to data by optimizing over k values (Figure 10). For experimental dose-response curves in which the steepness falls within the limits on n indicated in Figure 9 (approximately less than 3.75), we find that curves are fit well (Doxycycline, Spectinomycin, Streptomycin, Chloramphenicol, and Fusidic Acid). However, for sharp curves (panel Gentamicin, Amikacin, Tobramycin, Erythromycin, and Spiramycin) we find that the theoretical model is not able to fit the data as well. It is possible that this can be resolved by optimizing simultaneously over k and D.

We also find that k and D both decrease exponentially with the $EC50$, the antibiotic concentration at which growth is inhibited to 50%, the parameter fit from the curve fitting model as shown in Panel 10B. Additionally, this also indicates that the relationship between k and D can be approximated as linear, and increasing k is equivalent to increasing D. Therefore the term of interest is kD. Figures 10C and D show the distributions of k and D, which are left-skewed. The isolated points on the right are likely to be biologically meaningful, because the curves are all fit relatively well. Additionally, the relationship between $EC50$ and both of the free parameters is exponentially decreasing both when the curve-fitting algorithm is run on the to theoretical dose-response curves for a range of k and D values (Figures 9 C and D) and on data (Figure 10B). The variation in the distribution is likely due to shifts in antibiotic specific diffusion or ribosome binding rates. A wider analysis can be done in the future by fitting all of the experimental dose response curves of ribosome targeting antibiotics across species, and analyzing the variation of optimal parameter values within and across antibiotics.

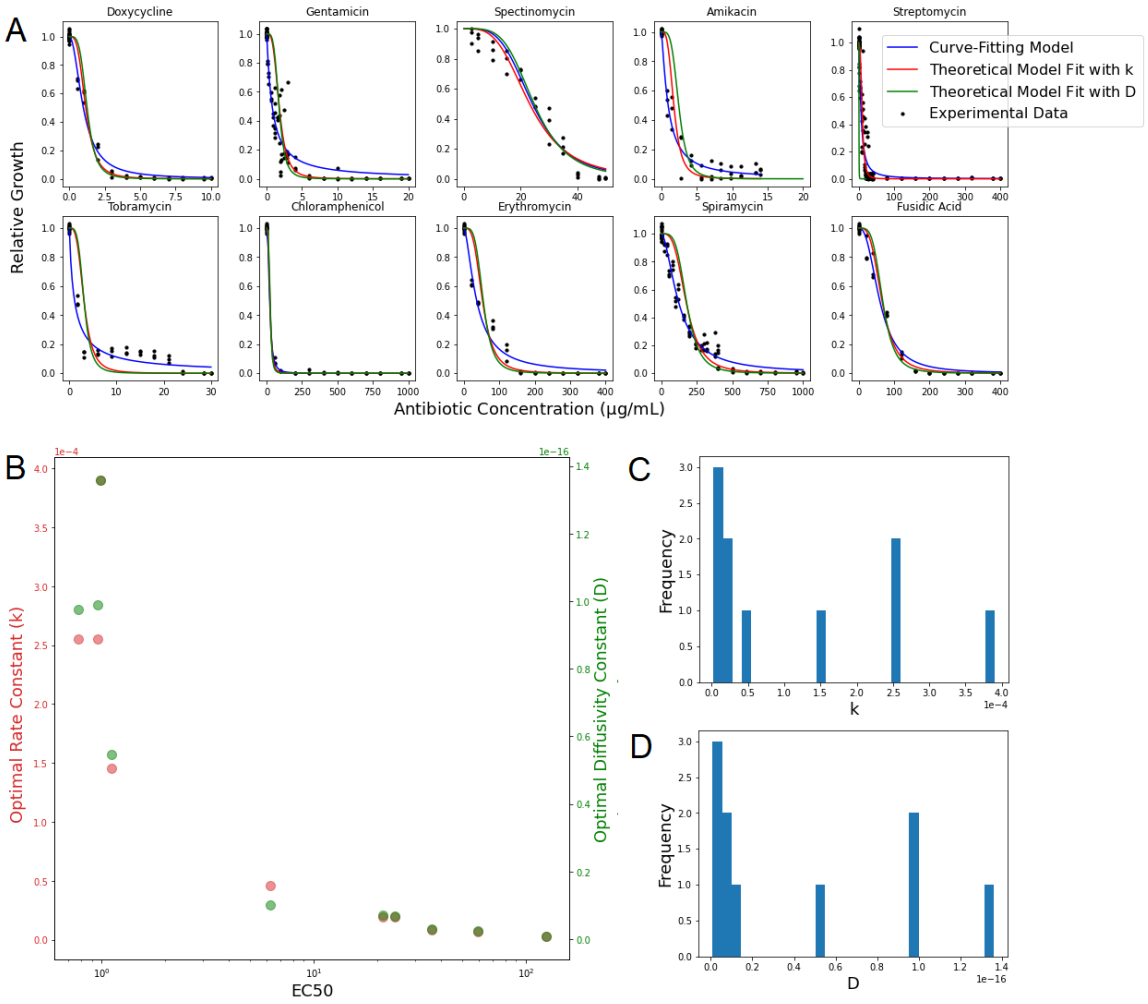

Figure 10: **Fitting the model to experimental data from *E. coli*** (A) Theoretical model fit to experimentally measured dose-response curves of *E. coli* and 10 ribosome-targeting antibiotics. The data is first fit an inverse-Hill function curve (blue) and then the theoretical model is fit to the blue curve by optimizing the free parameters in the models – k, the rate constant for antibiotic binding to ribosomes (blue line) or D, the diffusivity constant (green line). (B) The optimal k value (red), D value (green) decreases exponentially with the $EC50$ value that is fit to the data. (C) Histogram of k values. (D) Histogram of D values.

4.2 Theoretical Predictions of Size Dependent Trade-offs and Constraints

Our overarching goal is to make predictions of the relationship between cell size and susceptibility to ribosome targeting antibiotics. In order to do this we incorporate size-dependent shifts in cellular composition into the model described in Section 2.1 as outlined in Section 2.2. Cell size affects both the percentage volume of ribosomes and proteins (Figure 2A). The shift in the percentage volume of the protein pool affects the minimum number of ribosomes the cell must have under antibiotic stress, which affects (i) changes energetic costs and therefore the energy-limiting antibiotic concentration, and (ii) the volume of ribosome-antibiotic complexes, which contribute to the required dry volume of the cell, which cannot exceed total cell volume. Moreover, a cell that has a high dry volume fraction without antibiotic stress cannot tolerate the same increase in dry volume that a cell with low dry volume can. The effect of cell size on the volume-limiting antibiotic concentration is therefore compounded by the relationship between cell size and the percentage dry volume of the cell without antibiotic stress (shown in Figure 2B). Hence cell size determines both the energy-limiting and volume-limiting minimum inhibitory concentrations.

We examine the cell size dependent shifts in cellular composition under antibiotic stress by comparing the volume of ribosome, ribosome-antibiotic complexes, and the total dry volume at MIC_{95}, the concentration at which cell growth is inhibited to 5% due energetic limitations. The volume of other cellular components is assumed to be constant under antibiotic stress. Figure 11 shows that the the change in ribosome volume at the minimum inhibitory concentration is size-dependent, and that for smaller cell sizes the minimum ribosome volume increases under antibiotic stress, but that it increases at larger volumes. Additionally, the percentage of cell volume taken up by the ribosome-antibiotic complex at MIC_{95} (red in Fig. 11) decreases with increases in cell size. This drives the increase in total required dry volume (purple), which exceeds the cell volume at small cell sizes, indicating

that a limitations due to space within the cell are the limiting factor in these cell sizes rather than energetic limitations.

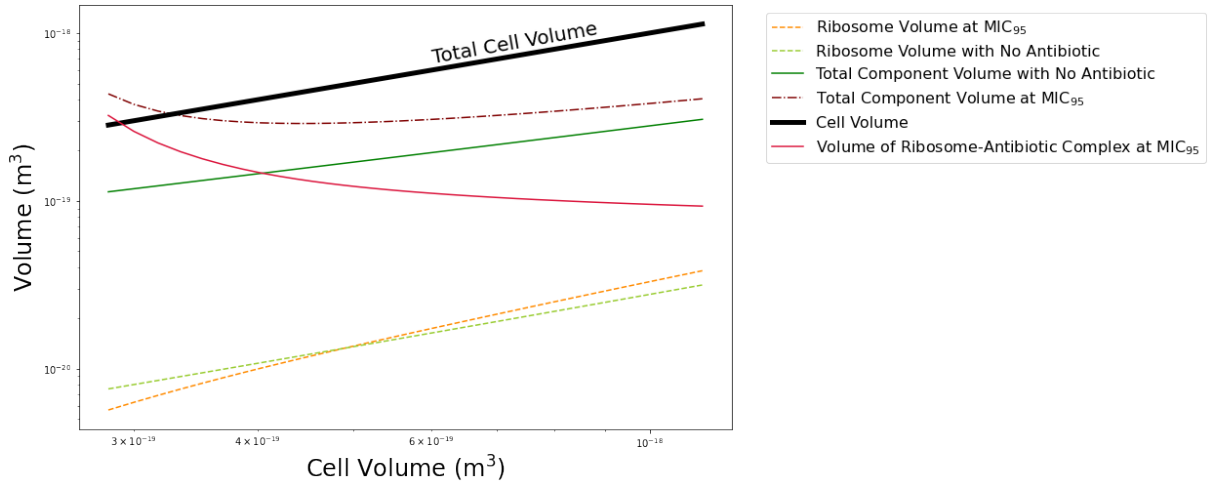

Figure 11: **Volumetric constraints on response to antibiotics** Cellular composition at MIC_{99} shifts based on cell size. Increases in the volume of ribosome-antibiotic complexes drives the increase in dry volume. For small cell sizes dry volume exceeds total cell volume at MIC_{99}, indicating that lower antibiotic concentrations would be inhibitory.

Our theoretical results thus far incorporating cellular composition, diffusion, energy budget, and constraints on dry volume suggest cell size affects the both the energy-limiting and volume-limiting inhibitory antibiotic concentrations. A comparison of these two concentrations shows that cell size does have an effect on theoretical predictions of both the energy-limiting and volume-limiting concentrations, as shown in Figure 12. The predicted energy limiting concentration, (blue) decreases sharply with cell size, whereas the predicted volume-limiting concentration increases with cell size. Interestingly, the two curves intersect, indicating that there is a trade-off between energy and volume limiting concentrations across cell sizes.

Additionally, we find that there is a strong power-law relationship (of the form $IC \propto V^{\alpha}$, where IC is an inhibitory concentration and V is cell volume) between cell volume and

both the energy-limiting and volume-limiting concentration. This is indicated by the linear nature of the two curves in Figure 12, on which both axes are log-scaled. When we fit a linear regression between log transformed cell volume and both the energy limiting antibiotic concentration and the volume-limiting antibiotic concentration we find high R^2 values of 0.993 and 0.998 respectively. The slopes from the linear regression can be used to find the exponent in the power-law relationship. Therefore we find that $MIC_e \propto V^{-1.35}$ and $MIC_v \propto V^{1.87}$.

The overall predicted inhibitory antibiotic concentration for a cell of a specified size is the minimum of MIC_e and MIC_v, i.e. the minimum of the two curves shows in Figure 12, because any one of these constraints can limit cell growth. Additionally, we model the case in which cells respond antibiotics by changing their cellular composition and resource distribution optimally, so our MIC predictions are actually upper bounds on inhibitory concentrations, and we expect that cells that do not respond optimally will have a lower MIC than indicated by the two curves in Figure 12. Therefore, we predict that experimentally measured minimum inhibitory concentrations will lie in the intersection of the blue and red shaded areas.

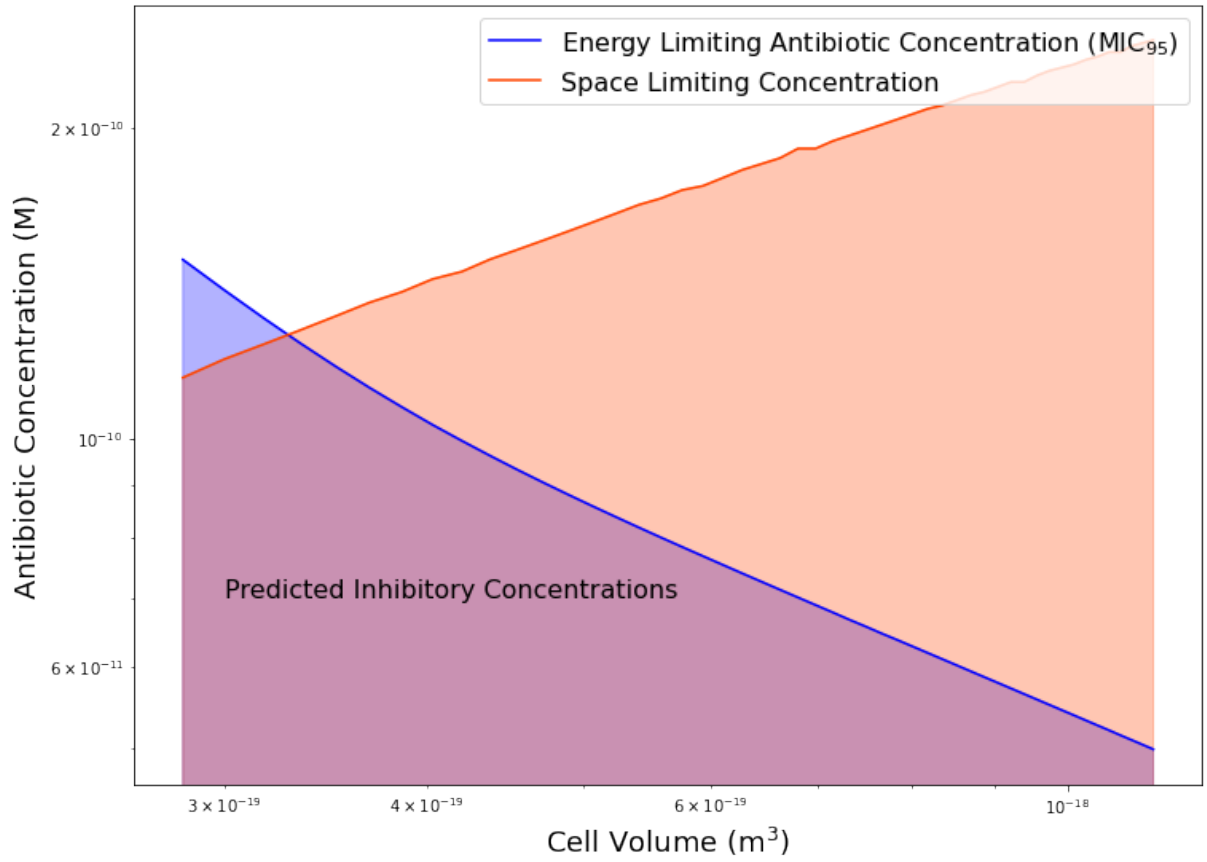

Figure 12: **Predicted energy and space limiting concentrations across species** Changes in the predicted inhibitory concentrations based on cell size are due to systematic shifts in cellular composition and surface area. The energy-limiting concentration (blue) is based on the energetics resulting from the macromolecular dynamics within the cell, and the space-limiting concentration (orange) is the antibiotic concentration at which the volume of the required components exceeds the total cell volume. The overall predicted inhibitory concentration is the minimum of the energy and volume limiting antibiotic concentrations. Because our model assumes that the cell responds optimally, the minimum of the two lines is an upper bound on the inhibitory concentration. Hence, the purple shaded region below the minimum of the two curves represents the predicted inhibitory concentrations.

4.3 Experimental Results

We measure detailed dose-response curves for 11 bacterial species and 24 antibiotics, 9 of which are ribosome-targeting, and 10 of which are cell wall targeting, as detailed in Section 3.1. Additionally, we measure dose-response to antibiotics that have been shown to have non-additive interactions with temperatures at sub-optimal temperatures. We find dose response curves as shown in Figure 4.3. We fit dose response curves 3.2 and estimate MIC_{95}, the antibiotic concentration at which growth is limited to 5% of the growth observed in positive controls. We then compare the MIC_{95} measured at the optimal temperature to the size measured using microscopy techniques.

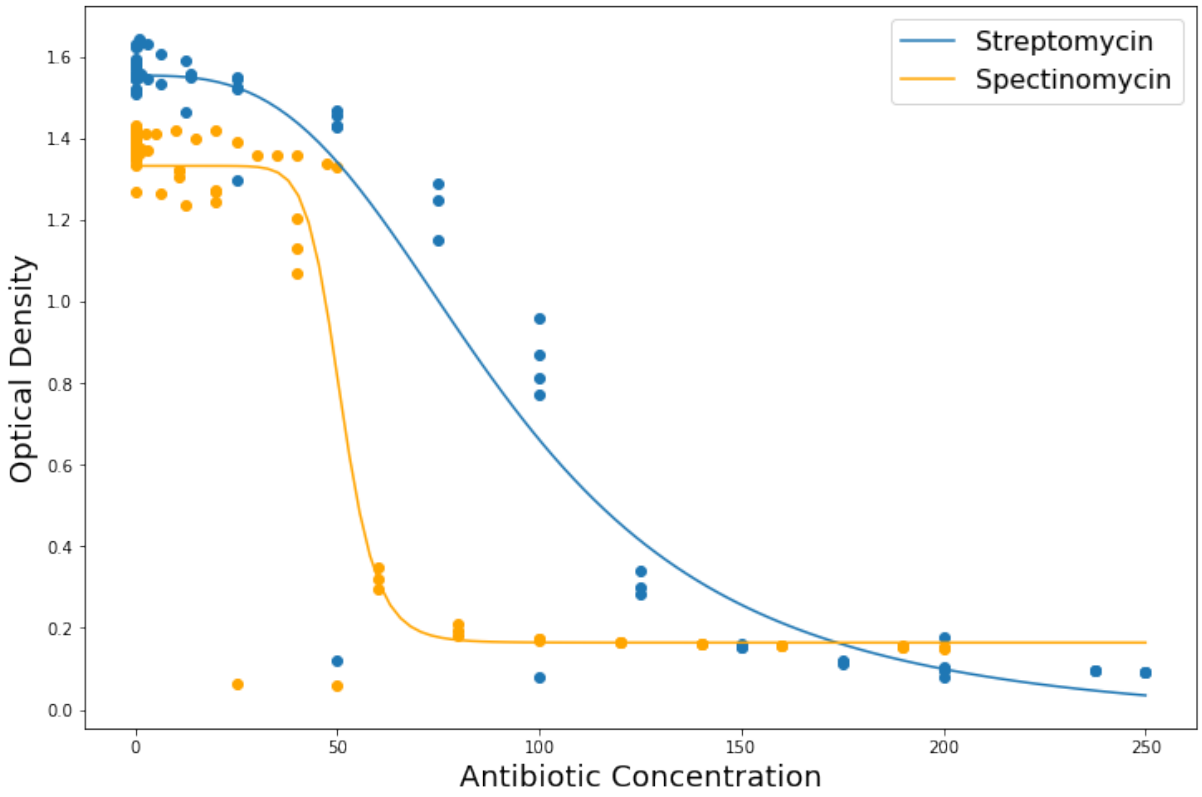

Figure 13: **Example dose-response data** Experimental dose-response curves of *Lactobacillus plantarum* in streptomycin (blue) and spectinomycin (orange)
which are fit to Eq. 17 using non-linear least squares. This is used to measure experimental minimum inhibitory concentrations.

Measured MIC_{95} values at optimal temperatures for 10 cell-wall targeting antibiotics and 9 ribosome-targeting antibiotics are shown in Figures 14 and 15. Panels in Figures 14 and 15 show the relationship between cell size and MIC_{95} for individual antibiotics. We note that for both cell wall and antibiotic targeting antibiotics mid-sized cells have higher MICs than larger and smaller cells, and we find no correlation between optimal growth temperatures and MIC for any of the panels shown below. In both cases, we find that data points fall below an envelope that peaks at mid-sized cells. In the plots in these two figures the y-axis is log-transformed, and the envelopes representing the upper bounds on MIC appear to be intersections of two lines, which qualitatively matches our theoretical predictions.

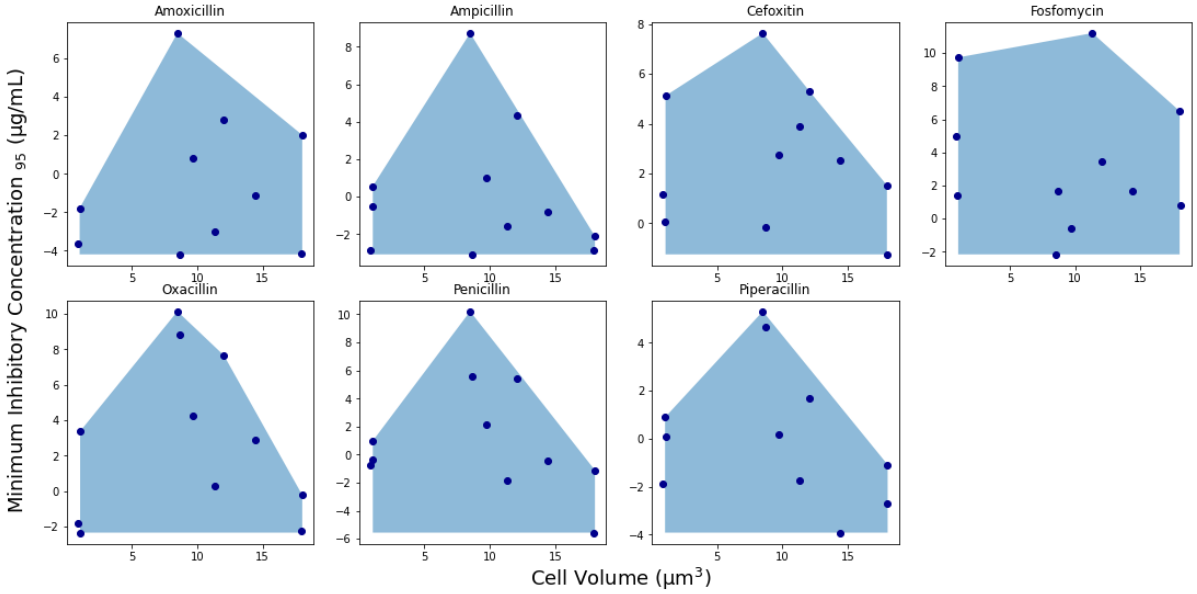

Figure 14: **Measured MIC_{95} for cell wall targeting antibiotics across species of different sizes** Log-MIC is presented for 7 cell-wall targeting antibiotics across species of varying cell sizes. The convex hull of the data points and the x-axis is shown, qualitatively matching the theoretical predictions of minimum inhibitory concentrations (in Figure 12)

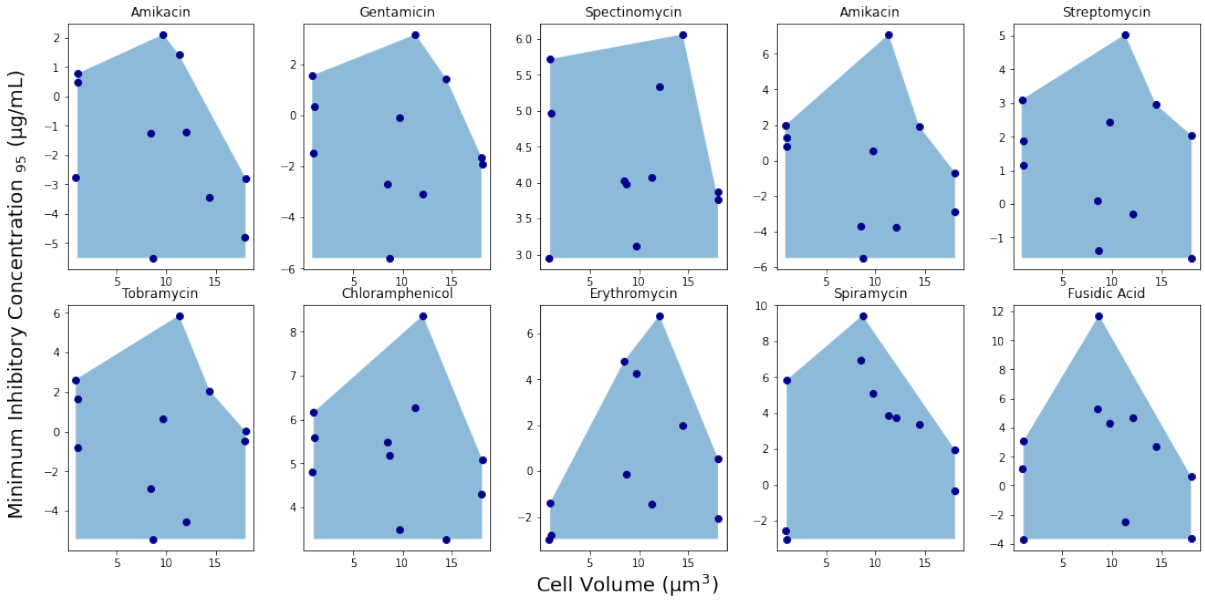

Figure 15: **Measured MIC_{95} for ribosome targeting antibiotics across species of different sizes** Log-MIC is presented for 10 ribosome targeting antibiotics across species of varying cell sizes. The convex hull of the data points and the x-axis is shown, qualitatively matching the theoretical predictions of minimum inhibitory concentrations (in Figure 12)

5 Discussion

We are able to derive a model that can be fit to experimentally measured dose-response curves and that can make predictions of antibiotic susceptibility across species based on cell size. We identify two limiting constraints to cell growth with antibiotics – increased metabolic expenditure due to degradation of antibiotic targets, and a decrease in space available in the cell due to increased dry volume under antibiotic stress. Trade-offs between these two constraints lead to theoretical predictions that mid-sized cells are least susceptible to ribosome-targeting antibiotics. Our theoretical prediction is matched qualitatively by our experimental results that minimum inhibitory concentrations of ribosome-targeting antibiotics are observed to be higher in mid-sized cells than extremely large or small cells.

Furthermore, we observe the same trend in cell-wall targeting antibiotics, suggesting that the underlying trade-offs between multiple constraints such as cellular energetics and volume limitations could drive size-based trends in antibiotic susceptibility.

The coarse-grained model that we present here captures is able to capture several essential processes involved in bacterial inhibition by antibiotic, including the disruption of translation by ribosome-targeting antibiotics and the optimal resource reallocation that can be done by a cell, and connects this to growth rates, which can be measured experimentally. We make several assumptions in the model, including the irreversible binding of the antibiotic to the target and the partitioning of mRNA transcripts between ribosomal and non-ribosomal transcripts (γ) being constant across the cell cycle. Additionally, we assume that the cell does not reduce the size of its protein pool under antibiotic stress. These simplifying assumptions allow us to make analytic calculations that approximate the behavior of the cell under antibiotic stress.

Our model leads to insights on the complexity of re-calibration of resources such as the proportion of ribosomal transcripts and number of ribosomes, and connects different strategies explicitly to energetic costs (Figure 8). Additionally, we identify two limitations on cell growth - energetic costs and volume limitation. While the model presented here is specific to ribosome-targeting antibiotics, the general framework connecting optimal macromolecular dynamics to energy limitations, volumetric constraints, and cell growth can be applied widely to other antibiotic classes, and more broadly to other stressors.

By incorporating cell-size dependent shifts in cellular composition into the model for generating dose-response curves, we are able to make predictions of the maximum antibiotic concentrations that a cell can tolerate based on energy and volume limitations (Figure 12). The intersection of the curves representing the two limiting concentrations indicates that there is a trade-off between energy and volume constraints that cells must navigate in response to antibiotics. This creates regimes in cell sizes that are "energy-limited", where the

inhibitory concentration based on energetic factors is lower than the concentration based on volumetric constraints, and similarly a "volume-limited" regime. Therefore our theoretical framework suggests that cell size determines the limiting factors for cell growth under antibiotic stress. Our theoretical result that cells are volume-limited at larger cell sizes also suggest that increasing cell size under antibiotic treatment could be a strategy to mitigate volume-limitations in these size regimes.

Furthermore, in our analysis of cell-size dependent shifts in inhibitory antibiotic concentrations we find that the predictions of the energetic and molecular inhibitory concentrations can be approximated by power-laws. Power laws fit data generated from out model extremely well, with an R^2 value over 0.99 in linear regressions of the log transformed cell size and log transformed minimum inhibitory concentration. (Figure 12). We note that there is upwards curvature in the energy-limiting antibiotic concentration, indicating that power-laws are able to approximate this trend well, especially at large cell sizes, but that there are complex underlying processes that lead to this relationship that are not captured by the power-law relationship. While cell-size dependency in the model is based upon the power-law approximation of protein volume in cells, the prediction of inhibitory antibiotic concentrations is complicated by several factors such as cell-size dependencies in growth rates, resource redistribution, and volumetric limitations on total cell component volume, which does not follow a power-law. Power laws have been observed in several contexts, biological and otherwise [34]. Our findings indicate that such power-law relationships are also of relevance in the context of antibiotic stress response in bacteria.

Our model assumes that cells respond optimally and therefore it predicts upper bounds on inhibitory concentrations, so we expect experimentally measured data points to fall below our predictions. Additionally, bacterial species might deviate in the cell-size dependent composition that is predicted in Kempes *et al* [4], which may also result in deviations from our predicted results. Because the predictions of cellular composition as a function of cell

size are based on energetic optimality, deviation from predicted cellular composition could also result in a lower minimum inhibitory concentration than predicted. Measurements in this case would also fall under the upper bound on inhibitory concentrations that we predict.

Our experimental measurements of antibiotic susceptibility are matched qualitatively by our model. The dose-response curves generated by our model are similar to empirically measured dose-response curves. We are able to fit a our model to a range of dose-response curves based on free parameters k, the antibiotic-specific rate constant that represents that rate at which an antibiotic molecule binds to a target component, and D, the diffusivity constant representing the rate at which the antibiotic moves across the cellular envelope, as shown in Figure 10. However, fitting empirical data is limited by the range of curves that our model is able to produce and our understanding of the interactions between the free parameters and cell size. This is an area for future work.

Moreover, our empirical measurements of minimum inhibitory concentrations across cell size qualitatively match our theoretical predictions that mid-sized cells are least susceptible to antibiotics, and therefore have the highest inhibitory concentrations. Because we measure inhibitory concentrations across the same 11 species, it is possible that their minimum inhibitory concentrations are correlated, especially within groups of antibiotics, and we find that this is especially true in the case of cell-wall targeting antibiotics (Figure 14). This indicates that response to antibiotics is highly dependent on the mechanism of action, and that response to antibiotics should be modeled based on their mechanism of action, as we do here.

Our theoretical and experimental results together suggest that cell size could play a role in antibiotic stress response, and ultimately in the evolution of antibiotic resistance. We find that cells must deal with multiple constraints such as energy and volume limitations and that the limiting constraint could depend on cell-size. Future work measuring the response of cells under antibiotic stress, in particular shifts in molecular composition and cell size in bacteria

exposed to antibiotics, could be used to check assumptions in our modeling framework, and explain our theoretical and experimental results. Additionally, we only address the response of wild-type strains to antibiotics, and future studies linking cell size with the evolution of antibiotic resistance could be used as the basis for strategies to combat antibiotic resistance.

References

[1] W. H. Organization, Ed., *Antimicrobial resistance: global report on surveillance*, en. Geneva, Switzerland: World Health Organization, 2014, OCLC: ocn880847527, ISBN: 978-92-4-156474-8.

[2] "Antibiotic resistance threats in the united states," 2013. [Online]. Available: http://www.cdc.gov/drugresistance/threat-report-2013/pdf/ar-threats-2013-508.pdf.

[3] C. P. Kempes, P. M. van Bodegom, D. Wolpert, E. Libby, J. Amend, and T. Hoehler, "Drivers of bacterial maintenance and minimal energy requirements," *Frontiers in Microbiology*, vol. 8, p. 31, 2017, ISSN: 1664-302X. DOI: 10.3389/fmicb.2017.00031. [Online]. Available: https://www.frontiersin.org/article/10.3389/fmicb.2017.00031.

[4] C. P. Kempes, L. Wang, J. P. Amend, J. Doyle, and T. Hoehler, "Evolutionary tradeoffs in cellular composition across diverse bacteria," *ISME J*, vol. 10, pp. 2145–2157, 2016. DOI: 10.1038/ismej.2016.21.

[5] S. Vijay, R. R. Nair, D. Sharan, K. Jakkala, N. Mukkayyan, S. Swaminath, A. Pradhan, N. V. Joshi, and P. Ajitkumar, "Mycobacterial cultures contain cell size and density specific sub-populations of cells with significant differential susceptibility to antibiotics, oxidative and nitrite stress," *Frontiers in Microbiology*, vol. 8, p. 463, 2017, ISSN: 1664-302X. DOI: 10.3389/fmicb.2017.00463. [Online]. Available: https://www.frontiersin.org/article/10.3389/fmicb.2017.00463.

[6] B. B. Aldridge, M. Fernandez-Suarez, D. Heller, V. Ambravaneswaran, D. Irimia, M. Toner, and S. M. Fortune, "Asymmetry and aging of mycobacterial cells lead to variable growth and antibiotic susceptibility," *Science*, vol. 335, no. 6064, pp. 100–104, 2012, ISSN: 0036-8075. DOI: 10.1126/science.1216166. eprint: https://science.

sciencemag.org/content/335/6064/100.full.pdf. [Online]. Available: https://science.sciencemag.org/content/335/6064/100.

[7] L. C. Gomes, L. N. Silva, M. Simões, L. F. Melo, and F. J. Mergulhão, "Escherichia coli adhesion, biofilm development and antibiotic susceptibility on biomedical materials," *Journal of Biomedical Materials Research Part A*, vol. 103, no. 4, pp. 1414–1423, 2015. DOI: https://doi.org/10.1002/jbm.a.35277. eprint: https://onlinelibrary.wiley.com/doi/pdf/10.1002/jbm.a.35277. [Online]. Available: https://onlinelibrary.wiley.com/doi/abs/10.1002/jbm.a.35277.

[8] M. Scott and T. Hwa, "Bacterial growth laws and their applications," eng, *Curr Opin Biotechnol*, vol. 22, no. 4, pp. 559–565, Aug. 2011, Edition: 2011/05/16, ISSN: 1879-0429. DOI: 10.1016/j.copbio.2011.04.014. [Online]. Available: https://pubmed.ncbi.nlm.nih.gov/21592775.

[9] M. Scott, S. Klumpp, E. M. Mateescu, and T. Hwa, "Emergence of robust growth laws from optimal regulation of ribosome synthesis," *Molecular Systems Biology*, vol. 10, no. 8, p. 747, Aug. 2014, Publisher: John Wiley & Sons, Ltd, ISSN: 1744-4292. DOI: 10.15252/msb.20145379. [Online]. Available: https://www.embopress.org/doi/full/10.15252/msb.20145379 (visited on 06/11/2021).

[10] D. W. Erickson, S. J. Schink, V. Patsalo, J. R. Williamson, U. Gerland, and T. Hwa, "A global resource allocation strategy governs growth transition kinetics of Escherichia coli," en, *Nature*, vol. 551, no. 7678, pp. 119–123, Nov. 2017, Number: 7678 Publisher: Nature Publishing Group, ISSN: 1476-4687. DOI: 10.1038/nature24299. [Online]. Available: https://www.nature.com/articles/nature24299 (visited on 06/11/2021).

[11] M. Zhu and X. Dai, "Growth suppression by altered (p)ppGpp levels results from non-optimal resource allocation in Escherichia coli," *Nucleic Acids Research*, vol. 47,

no. 9, pp. 4684–4693, May 2019, ISSN: 0305-1048. DOI: 10.1093/nar/gkz211. [Online]. Available: https://doi.org/10.1093/nar/gkz211 (visited on 06/11/2021).

[12] J. Monod, "The growth of bacterial cultures," *Annual Review of Microbiology*, vol. 3, no. 1, pp. 371–394, 1949. DOI: 10.1146/annurev.mi.03.100149.002103. eprint: https://doi.org/10.1146/annurev.mi.03.100149.002103. [Online]. Available: https://doi.org/10.1146/annurev.mi.03.100149.002103.

[13] M. Schaechter, O. MaalØe, and N. O. Kjeldgaard, "Dependency on Medium and Temperature of Cell Size and Chemical Composition during Balanced Growth of Salmonella typhimurium," *Microbiology*, vol. 19, no. 3, pp. 592–606, 1958, Publisher: Microbiology Society Type: Journal Article, ISSN: 1465-2080. DOI: https://doi.org/10.1099/00221287-19-3-592. [Online]. Available: https://www.microbiologyresearch.org/content/journal/micro/10.1099/00221287-19-3-592.

[14] P. Greulich, J. Doležal, M. Scott, M. R. Evans, and R. J. Allen, "Predicting the dynamics of bacterial growth inhibition by ribosome-targeting antibiotics," eng, *Phys Biol*, vol. 14, no. 6, pp. 065 005–065 005, Nov. 2017, ISSN: 1478-3975. DOI: 10.1088/1478-3975/aa8001. [Online]. Available: https://pubmed.ncbi.nlm.nih.gov/28714461.

[15] C. P. Kempes, S. Dutkiewicz, and M. J. Follows, "Growth, metabolic partitioning, and the size of microorganisms," *Proceedings of the National Academy of Sciences*, vol. 109, no. 2, pp. 495–500, 2012, Publisher: National Academy of Sciences _eprint: https://www.pnas.org/content/109/2/495.full.pdf, ISSN: 0027-8424. DOI: 10.1073/pnas.1115585109. [Online]. Available: https://www.pnas.org/content/109/2/495.

[16] J. Cama, A. M. Henney, and M. Winterhalter, "Breaching the Barrier: Quantifying Antibiotic Permeability across Gram-negative Bacterial Membranes," *Journal of Molecular Biology*, vol. 431, no. 18, pp. 3531–3546, 2019, ISSN: 0022-2836. DOI: https:

//doi.org/10.1016/j.jmb.2019.03.031. [Online]. Available: https://www.sciencedirect.com/science/article/pii/S0022283619301810.

[17] D. Serbanescu, N. Ojkic, and S. Banerjee, "Nutrient-Dependent Trade-Offs between Ribosomes and Division Protein Synthesis Control Bacterial Cell Size and Growth," *Cell Reports*, vol. 32, no. 12, p. 108 183, 2020, ISSN: 2211-1247. DOI: https://doi.org/10.1016/j.celrep.2020.108183. [Online]. Available: https://www.sciencedirect.com/science/article/pii/S2211124720311724.

[18] S. Hui, J. M. Silverman, S. S. Chen, D. W. Erickson, M. Basan, J. Wang, T. Hwa, and J. R. Williamson, "Quantitative proteomic analysis reveals a simple strategy of global resource allocation in bacteria," *Molecular Systems Biology*, vol. 11, no. 2, p. 784, 2015. DOI: https://doi.org/10.15252/msb.20145697. eprint: https://www.embopress.org/doi/pdf/10.15252/msb.20145697. [Online]. Available: https://www.embopress.org/doi/abs/10.15252/msb.20145697.

[19] P. Fernandes, "Fusidic Acid: A Bacterial Elongation Factor Inhibitor for the Oral Treatment of Acute and Chronic Staphylococcal Infections," *Cold Spring Harb Perspect Med*, vol. 6, no. 1, Jan. 2016, ISSN: 2157-1422. DOI: 10.1101/cshperspect.a025437. [Online]. Available: https://www.ncbi.nlm.nih.gov/pmc/articles/PMC4691801/ (visited on 06/09/2021).

[20] G. Kapoor, S. Saigal, and A. Elongavan, "Action and resistance mechanisms of antibiotics: A guide for clinicians," *J Anaesthesiol Clin Pharmacol*, vol. 33, no. 3, pp. 300–305, 2017, ISSN: 0970-9185. DOI: 10.4103/joacp.JOACP_349_15. [Online]. Available: https://www.ncbi.nlm.nih.gov/pmc/articles/PMC5672523/ (visited on 06/09/2021).

[21] L. Luzzatto, D. Apirion, and D. Schlessinger, "Mechanism of action of streptomycin in E. coli: Interruption of the ribosome cycle at the initiation of protein synthesis.," *Proc*

Natl Acad Sci U S A, vol. 60, no. 3, pp. 873–880, Jul. 1968, ISSN: 0027-8424. [Online]. Available: https://www.ncbi.nlm.nih.gov/pmc/articles/PMC225133/ (visited on 06/09/2021).

[22] R. S. Edson and C. L. Terrell, "The aminoglycosides," eng, *Mayo Clin Proc*, vol. 74, no. 5, pp. 519–528, May 1999, ISSN: 0025-6196. DOI: 10.4065/74.5.519.

[23] T. Okamoto, H. Yoshiyama, T. Nakazawa, I.-D. Park, M.-W. Chang, H. Yanai, K. Okita, and M. Shirai, "A change in PBP1 is involved in amoxicillin resistance of clinical isolates of Helicobacter pylori," eng, *J Antimicrob Chemother*, vol. 50, no. 6, pp. 849–856, Dec. 2002, ISSN: 0305-7453. DOI: 10.1093/jac/dkf140.

[24] J. Birnbaum, E. O. Stapley, A. K. Miller, H. Wallick, D. Hendlin, and H. B. Woodruff, "Cefoxitin, a semi-synthetic cephamycin: A microbiological overview," *Journal of Antimicrobial Chemotherapy*, vol. 4, no. suppl_B, pp. 15–32, Jan. 1978, ISSN: 0305-7453. DOI: 10.1093/jac/4.suppl_B.15. [Online]. Available: https://doi.org/10.1093/jac/4.suppl_B.15 (visited on 06/09/2021).

[25] *Ciprofloxacin: Chemistry, Mechanism of Action, Resistance, Antimicrobial Spectrum, Pharmacokinetics, Clinical Trials, and Adverse Reactions - LeBel - 1988 - Pharmacotherapy: The Journal of Human Pharmacology and Drug Therapy - Wiley Online Library*. [Online]. Available: https://accpjournals.onlinelibrary.wiley.com/doi/abs/10.1002/j.1875-9114.1988.tb04058.x?casa_token=ReGka8w35-sAAAAA:wOnEnRWuh0ghVFjve7NSofpHM78kK4E5vhvK0ravbs6DEaDFUMYlFoYsvYg1xfgRxYAefSmyDBOOCO4 (visited on 06/09/2021).

[26] J. Spížek and T. Řezanka, "Lincomycin, clindamycin and their applications," en, *Appl Microbiol Biotechnol*, vol. 64, no. 4, pp. 455–464, May 2004, ISSN: 1432-0614. DOI: 10.1007/s00253-003-1545-7. [Online]. Available: https://doi.org/10.1007/s00253-003-1545-7 (visited on 06/09/2021).

[27] F. E. Hahn and S. G. Sarre, "Mechanism of Action of Gentamicin," *The Journal of Infectious Diseases*, vol. 119, no. 4/5, pp. 364–369, 1969, Publisher: Oxford University Press, ISSN: 0022-1899. [Online]. Available: https://www.jstor.org/stable/30102364 (visited on 06/09/2021).

[28] F. L. Goffic, M.-L. Capmau, F. Tangy, and M. Baillarge, "Mechanism of Action of Aminoglycoside Antibiotics," en, *European Journal of Biochemistry*, vol. 102, no. 1, pp. 73–81, 1979, _eprint: https://febs.onlinelibrary.wiley.com/doi/pdf/10.1111/j.1432-1033.1979.tb06264.x, ISSN: 1432-1033. DOI: 10.1111/j.1432-1033.1979.tb06264.x. [Online]. Available: https://febs.onlinelibrary.wiley.com/doi/abs/10.1111/j.1432-1033.1979.tb06264.x (visited on 06/09/2021).

[29] R. Davis and H. M. Bryson, "Levofloxacin," en, *Drugs*, vol. 47, no. 4, pp. 677–700, Apr. 1994, ISSN: 1179-1950. DOI: 10.2165/00003495-199447040-00008. [Online]. Available: https://doi.org/10.2165/00003495-199447040-00008 (visited on 06/09/2021).

[30] G. R. Hartmann, P. Heinrich, M. C. Kollenda, B. Skrobranek, M. Tropschug, and W. Weiß, "Molecular Mechanism of Action of the Antibiotic Rifampicin," en, *Angewandte Chemie International Edition in English*, vol. 24, no. 12, pp. 1009–1014, 1985, _eprint: https://onlinelibrary.wiley.com/doi/pdf/10.1002/anie.198510093, ISSN: 1521-3773. DOI: 10.1002/anie.198510093. [Online]. Available: https://onlinelibrary.wiley.com/doi/abs/10.1002/anie.198510093 (visited on 06/09/2021).

[31] N. Tanaka, "Mechanism of Action of Aminoglycoside Antibiotics," en, in *Aminoglycoside Antibiotics*, ser. Handbook of Experimental Pharmacology, H. Umezawa and I. R. Hooper, Eds., Berlin, Heidelberg: Springer, 1982, pp. 221–266, ISBN: 978-3-642-68579-8. DOI: 10.1007/978-3-642-68579-8_5. [Online]. Available: https://doi.org/10.1007/978-3-642-68579-8_5 (visited on 06/09/2021).

[32] A. Brisson-Noël, P. Trieu-Cuot, and P. Courvalin, "Mechanism of action of spiramycin and other macrolides," *Journal of Antimicrobial Chemotherapy*, vol. 22, no. Supplement_B, pp. 13–23, Jul. 1988, ISSN: 0305-7453. DOI: 10.1093/jac/22.Supplement_B.13. [Online]. Available: https://doi.org/10.1093/jac/22.Supplement_B.13 (visited on 06/09/2021).

[33] M. D. Giambattista, Y. Engelborghs, E. Nyssen, and C. Cocito, "Kinetics of binding of macrolides, lincosamides, and synergimycins to ribosomes.," *Journal of Biological Chemistry*, vol. 262, no. 18, pp. 8591–8597, 1987, ISSN: 0021-9258. DOI: https://doi.org/10.1016/S0021-9258(18)47454-6. [Online]. Available: https://www.sciencedirect.com/science/article/pii/S0021925818474546.

[34] R. V. Solé, S. A. Levin, J. H. Brown, V. K. Gupta, B.-L. Li, B. T. Milne, C. Restrepo, and G. B. West, "The fractal nature of nature: Power laws, ecological complexity and biodiversity," *Philosophical Transactions of the Royal Society of London. Series B: Biological Sciences*, vol. 357, no. 1421, pp. 619–626, May 2002, Publisher: Royal Society. DOI: 10.1098/rstb.2001.0993. [Online]. Available: https://royalsocietypublishing.org/doi/abs/10.1098/rstb.2001.0993 (visited on 06/07/2021).